

# **3D MODELLING OF SLUMS USING TERRESTRIAL IMAGERY**

Linus Kihara Mwangi  
February, 2016

SUPERVISORS:  
Dr. Markus Gerke  
Dr. Francesco Nex





# 3D MODELLING OF SLUMS USING TERRESTRIAL IMAGERY

Linus Kihara Mwangi  
Enschede, The Netherlands, February, 2016

Thesis submitted to the Faculty of Geo-Information Science and Earth Observation of the University of Twente in partial fulfilment of the requirements for the degree of Master of Science in Geo-information Science and Earth Observation.  
Specialization: MSc. Geoinformatics

## SUPERVISORS:

Dr. Markus Gerke  
Dr. Francesco Nex

## THESIS ASSESSMENT BOARD:

Prof.Dr.Ir. M.G. Vosselman (Chair)  
Dr. R.V. Sliuzas (External Examiner)  
Dr. Markus Gerke  
Dr. Francesco Nex

#### DISCLAIMER

This document describes work undertaken as part of a programme of study at the Faculty of Geo-Information Science and Earth Observation of the University of Twente. All views and opinions expressed therein remain the sole responsibility of the author, and do not necessarily represent those of the Faculty.

## ABSTRACT

Terrestrial image based modelling (IBM) is a low cost method of creating 3D models of structures. It is currently a common application especially in architectural and archaeology fields. However, it has not been widely used in the field of cadastral survey and mapping. Many methods of 3D modelling such as LIDAR, require initial high costs in both software and hardware. Terrestrial IBM only requires a good quality camera, in terms of hardware, which is relatively cheap.

In this research, we look at the application of terrestrial IBM for creating a point cloud and delineation of a 2D outline of buildings in a slum environment in Nairobi. We begin with the development of good image acquisition practices in such a complex environment. The research then addresses the creation of the point clouds from structure from motion and dense image matching. The issue of scaling errors is later addressed by reference measurements.

Later, the co-registration of different point clouds into one model is addressed. Considering the complexity of the environment, images contain a lot of clutter and thus the point clouds are noisy implying a different approach must be used to co-register the models.

Quality assessment of the point clouds and laser measurements is done using reference data at the University of Twente, Enschede, because of the availability of reference data as compared to Nairobi. Some quality checks are also done on the Nairobi data.

Finally, a 2D footprint of the slum from the point cloud is created, which can serve as a cadastre.

**Keywords:** *Structure from motion, Point cloud, Registration of point clouds, Image based Modelling*

## ACKNOWLEDGEMENTS

Firstly, I would like to thank my supervisors Dr. Markus Gerke and Dr. Francesco Nex for all the advice, time and invaluable input they gave me. This research would not have been possible without the guidance, support, insight and expertise they provided.

I would also like to thank the entire ITC staff and family, for all I have learnt here and all the support they have offered as I was undertaking my studies.

Sincere gratitude to Pamoja Trust staff and the people of Mashimoni village for all the help they provided during my data acquisition.

I would also like to thank the Ministry of Land, Housing and Urban development in Kenya for nominating me for a scholarship and granting me study leave to pursue my Masters.

I would also like to thank the Dutch Government for granting me the Nuffic scholarship to study at ITC. I am forever grateful to have received this opportunity.

Finally, I would like to say a special thanks to my family and friends for their support and encouragement.

---

# TABLE OF CONTENTS

---

ABSTRACT.....	i
ACKNOWLEDGEMENTS.....	ii
LIST OF FIGURES .....	iv
LIST OF TABLES.....	v
LIST OF ABBREVIATIONS .....	vi
1. INTRODUCTION.....	1
1.1. Background.....	1
1.2. Motivation and Problem statement.....	2
1.3. Research Identification.....	3
1.3.1. Main objective .....	3
1.3.2. Specific objectives and research questions.....	3
1.4. Innovation aimed at.....	4
2. LITERATURE REVIEW.....	5
2.1. Image acquisition.....	6
2.2. Image Orientation .....	6
2.3. Point cloud reconstruction .....	7
2.4. Reference data.....	8
2.5. Co-registering the point clouds.....	9
2.5.1. Principal Component Analysis (PCA).....	9
2.5.2. Singular Value Decomposition (SVD) .....	10
2.5.3. Iterative Closest Point (ICP).....	11
3. METHODOLOGY.....	13
3.1. Datasets .....	13
3.1.1. Area of study.....	13
3.1.2. Data.....	14
3.1.3. Equipment.....	15
3.2. Image acquisition.....	17
3.3. Creating a Point cloud .....	18
3.4. Co-registration of the point clouds .....	19
3.4.1. Basic steps of the registration workflow .....	19
3.5. Creation of a 2D outline .....	21
3.6. Quality assessment of 2D and point clouds .....	22
3.7. Quality analysis of Spike laser measurement device.....	23
4. RESULTS AND DISCUSSIONS .....	25
4.1. Creation of point clouds .....	25
4.1.1. University of Twente models.....	25
4.1.2. Mashimoni Dataset.....	31
4.2. Automatic registration of point clouds.....	35
4.2.1. Registration using corresponding points (Rough registration).....	36
4.2.2. Registration using ICP .....	37
4.2.3. Correction of model using 2D control points from the orthophoto.....	37
4.2.4. Correction of heights using digital elevation model.....	38
4.3. Visualization of the point cloud.....	40
4.4. 2D footprint of the slum.....	41
4.5. Spike laser measuring device accuracy analysis .....	43
5. CONCLUSIONS AND RECOMMENDATIONS.....	49
5.1. Conclusions .....	49
5.1.1. Answers to research questions.....	49
5.2. Recommendations.....	51
LIST OF REFERENCES.....	53
APPENDICES .....	55
Appendix 1: Schuur Building at the UT.....	55
Appendix 2: Comparison of 2D GCPs and 3D GCPs.....	56
Appendix 3: Spike measurements .....	56
Appendix 4: Matlab Script for transformation.....	58

---

## LIST OF FIGURES

---

Figure 2.1: Epipolar geometry.....	7
Figure 2.2: Relationship between corresponding points on two point clouds.....	10
Figure 3.1(a): Mashimoni village, Nairobi.....	13
Figure 3.2: Spike laser device mounted on an iPad®.....	15
Figure 3.3: Time of flight principle.....	16
Figure 3.4: Sample measurement made using spike laser device.....	16
Figure 3.5: Image acquisition along corridors.....	17
Figure 3.6: Image acquisition method of buildings at University campus.....	18
Figure 3.7: Co-registration of point cloud.....	19
Figure 3.8: Image properties in Pix4D.....	20
Figure 3.9: Registration of point clouds workflow.....	21
Figure 3.10: 2D extraction from the 3D model and refinement in the overlapping images.....	22
Figure 3.11: Proposed methodology workflow.....	24
Figure 4.1: Point cloud including camera positions.....	25
Figure 4.2: Histogram of the Euclidean distance.....	27
Figure 4.3: (a) Scatter plot for bearing and (b) bearing of model points from the reference points derived from the RTK GPS point cloud: Both show random errors.....	27
Figure 4.4: Comparison of point cloud corrected with 2D GCPs (in black) with one corrected with 3D GCPs from RTK GPS (in red).....	28
Figure 4.5: (a) Scatter plot for bearing and (b) bearing of model points from the reference points: Both show random errors.....	29
Figure 4.6: Distribution of GCPs (shown as red crosses) in two buildings (a) Experiment 1 (b) Experiment 2.....	30
Figure 4.7: Sample point clouds.....	31
Figure 4.8: (a) Measurements done on the point cloud and refined in the multiview images (b) reference measurements done using the physical facade.....	32
Figure 4.9: (a) Measurements done on the point cloud (b) Corresponding measurement done on the orthophoto.....	34
Figure 4.10: (a) Registration errors shown on the point cloud (b) Registration errors shown on the 2D model.....	35
Figure 4.11: (a) Overlapping area between two point clouds showing the registration differences (b) Segmented area of the overlap.....	36
Figure 4.12: Corresponding points of the point clouds using point picking (rough registration).....	36
Figure 4.13: Aligned overlap area.....	36
Figure 4.14: Corresponding points in orthophoto and point cloud.....	37
Figure 4.15: Elevation differences still persisted after the correction using 2DGCPs.....	38
Figure 4.16: Camera positions with the elevation errors.....	38
Figure 4.17: Camera positions corrected for height using elevation model.....	39
Figure 4.18: Full point cloud of study area; co-registered and merged.....	39
Figure 4.19: Scatter plot of initial elevation against computed elevation from DEM.....	40
Figure 4.20: 2D outline of the slum overlaid on orthophoto.....	41
Figure 4.21: Error vectors for x and y axes.....	42
Figure 4.22: Measurement of brick wall.....	43
Figure 4.23: Normal Q-Q plots of (a) bearing (b) distance to target.....	45
Figure 4.24: Scatter plots of (a) distance vs residuals (b) bearing vs residuals.....	46
Figure 4.25: Histograms showing residuals of (a) wooden surface (b) metallic surface.....	47
Figure 5.1: Point cloud of Schuur building.....	55
Figure 5.2: Comparison of 2D models.....	55
Figure 5.3: Wall facade measurement.....	56
Figure 5.4: Wooden surface measurements.....	57
Figure 5.5: Metallic surface measurements.....	57



---

## LIST OF TABLES

---

Table 3.1: Software and Hardware.....	15
Table 4.1: Building corner points using RTK GPS compared to L1 GPS.....	26
Table 4.2: Residual errors of model point cloud .....	26
Table 4.3: Comparison of area and perimeter.....	28
Table 4.4: Building corner points using RTK GPS compared to L1 GPS.....	29
Table 4.5: Comparison of area and perimeter.....	29
Table 4.6: Descriptions of datasets.....	31
Table 4.7: Comparison of measurements on orthophoto and merged point cloud.....	34
Table 4.8: Comparison of corresponding points in point cloud and orthophoto .....	41
Table 4.9: Geolocation errors from 2D checkpoints.....	42
Table 4.10: Residuals of Spike measurements.....	43

## LIST OF ABBREVIATIONS

---

IBM	Image Based Modelling
LiDAR	Light Detection and Ranging
SfM	Structure from Motion
SIFT	Scale Invariant Feature Transform
SURF	Speeded Up Robust Features
UT	University of Twente
RTK	Real Time Kinematic
GPS	Global Positioning System
GCPs	Ground Control Points
RANSAC	Random Sample Consensus
DoF	Degrees of Freedom
DEM	Digital Elevation Model

# 1. INTRODUCTION

## 1.1. Background

Image based modelling (IBM) can be defined as a method for creation of 3D models from a series of overlapping 2D images using the principle of stereo photogrammetry. 3D models can be point clouds or meshes, created from both passive and active sensors. Passive sensors such as IBM produce data that must be post processed into 3D information. On the other hand, active sensors (e.g. laser scanners/LiDAR) produce readily available 3D information (Remondino, 2011). The derived 3D point cloud can be used for visualization, measurements and other applications. 2D models can then be extrapolated from 3D models. The 2D models can be used for GIS applications including cadastral mapping.

Two methods of image acquisition are possible, namely aerial and terrestrial (close range photogrammetry) methods. Depending on the application required, either method can be used. In modelling building facades, terrestrial based methods are better than aerial based methods. Aerial methods are good if the roof information is needed (Joshi, 2014). In this research there is need to define building walls and extract individual buildings in order to derive a 2D outline/ footprint. Thus, façade information is necessary and thus terrestrial images are preferred.

One of the challenges in using terrestrial images in IBM modelling is solving scaling and shift problems in the 3D model. By using geotagged photos i.e. images that have GPS coordinates, we take a first step in solving these problems. The drawback is that the GPS in the cameras is of a single frequency (L1 only) resulting in low positional accuracy. Reference measures such as ground control points can be used to solve this by georeferencing the model. We can further solve the issues of scaling the model using reference measurements that can be done with a measuring tape, using ground control points or using a laser measurement device e.g. Ike Spike.

Slum mapping is a complex and challenging field especially in cadastral surveys. Many conventional methods are time consuming, expensive and labour intensive. In Nairobi, Kenya, a local non-governmental organisation (NGO), namely Informal City in conjunction with Pamoja Trust is currently working on mapping of slums to create cadastral records of their existence. To do so it is necessary to develop an alternative low cost method for mapping the slum. This is addressed in this research using terrestrial IBM.

## 1.2. Motivation and Problem statement

Slums are informal settlements in urban areas in developing countries. Mapping of these slums is almost non-existent and their cadastral plans are not available. These leaves the slum dwellers vulnerable to evictions as they have no legal documentation of the existence of the slums (Amnesty International, 2009). Mapping of these slums is therefore necessary to protect slum dwellers from evictions and for urban planning and slum upgrading. This can be addressed by using terrestrial IBM for creating 3D and 2D models of the slums.

In creating 2D and 3D models, various methods such as GPS, total stations and laser scanners (aerial and terrestrial) can be used. In this research, terrestrial IBM methods are chosen due to their advantages over the other methods. For instance, RTK GPS will have poor observations in between the corridors of the slums and is relatively expensive as compared to terrestrial IBM. Secondly, total stations requires a line of sight between instrument and target and it's mobility from station to station is slow. The latter method is thus time consuming and labour intensive. Lastly, IBM techniques has some advantages over laser based techniques in that; they are relatively cheap, they provide texture and are flexible, in terms of data acquisition; especially terrestrial images can be taken from multiple views (Li, Chen, & Baltsavias, 2008).

In this environment, image acquisition is quite challenging. This is due to the general characteristics of the slums that include narrow corridors, near impassable paths, crowded scenes among others. Thus, image acquisition of the area of interest has to be well planned and executed.

Depending on the size of the slum, the data acquisition can done on different days and times. This results in a block by block approach in data processing. This leads to differences in the parameters e.g. from different GPS readings of the inbuilt GPS in the camera resulting in registration differences (shifts) between the different point clouds. To create one point cloud of the entire area of interest, co-registration of the different point clouds has to be done.

To analyse the quality of the 3D point cloud, the relative accuracy and the absolute accuracy are addressed. For the relative accuracy, checks can be done within the model. Whereas for the absolute accuracy, reference data, such as cadastral maps, orthophotos and ground control points are required. For quality analysis, some images will be acquired at the University of Twente campus, 3D and 2D models will be created and reference data will be used to analyse the resulting models.

This research aims at developing a fast, low cost method of mapping of buildings using IBM methods. The main output of the research will be a 2D footprint of the buildings created by image based modelling from terrestrial images. This 2D model can be published as a WebGIS or CAD representation and can be used to map the slums or applications such as developing a cadastre.

This research will use the knowledge of modern IBM techniques to further research on techniques to create a 2D boundary of a slum area. Slum characteristics such as geometry and non-uniform layout of the structures is a big challenge and will be addressed. Several models will be created from the data and the issue of automatic co-registration of the sub blocks will be addressed. Lastly, the spatial component of IBM techniques i.e. the issue of georeferencing which is not usually addressed in computer vision techniques will be researched.

### **1.3. Research Identification**

#### **1.3.1. Main objective**

The main objective of this research is to develop a low cost method to create a 3D model and delineate a 2D footprint of buildings in a slum to act as the slum outline. This will be done using geotagged terrestrial images from a digital camera mounted with a low cost laser device used for scaling the model.

#### **1.3.2. Specific objectives and research questions**

1. To develop an appropriate approach for image acquisition.
  - How will the entire area of interest be captured?
  - Considering the complexity of the scene, how will the images capture all the details necessary for creating the models?
  
2. To create a 3D point cloud and mesh from the images.
  - How will a 3D model of the slum be created with data obtained over a period of time?
  - How will the issue of georeferencing into a global system be handled with the absence of ground control points?
  
3. To create a 2D model of the buildings in the area of interest
  - How can the 2D boundary of the slum be extracted from facades of the buildings, considering a problematic 3D model due to the characteristics of a slum?
  - How to establish an optimal approach when digitizing the 2D model from the 3D model or from multi-view images?
  - How will individual objects from the point clouds be extracted with high precision?

4. To perform quality assessment of both the 2D and 3D models
  - How to determine the geometric accuracy of the models?
  - How can ground control points and other reference data be used to quantify errors of the model?
5. To scale the 3D model using measurements taken by the Ike Spike laser device
  - How to determine the horizontal and vertical planes to be used for measurements?
  - How to determine the relative accuracy of the Ike spike device?
6. To develop a method for automatic co-registration of point clouds
  - How will the registration differences between the different point clouds be handled and then stitched together to one model?
  - How will the different point clouds be co-registered and merged into one model automatically?

#### **1.4. Innovation aimed at**

The innovation of this research is analysing the application of terrestrial based IBM methods in creating a 2D footprint of buildings in a slum. The research also aims to do an analysis of the accuracy and restrictions of using a new, low cost and fast approach, i.e. Ike Spike laser device, for scaling a 3D model and its application in IBM methods. Lastly, this research aims to develop a method of automatic co-registration of sub-blocks of the point clouds in the slum environment.

## 2. LITERATURE REVIEW

Image based modelling (IBM) has come a long way in recent years. 3D models are used in various applications including modelling buildings. Debevec, Taylor and Malik (1996) developed a hybrid method to model building facades by combining geometry based and image based approaches. The main drawbacks of this method was that, it was manually intensive in matching features and the intrinsic parameters of the camera had to be known. Using uncalibrated cameras, Liebowitz, Criminisi and Zisserman (1999) developed a method to reconstruct a 3D scenes using geometric constraints i.e. right angles, planar surfaces. This method's major limitation was that it could not reconstruct a model in structures with poor geometric relations and non-uniform surfaces e.g. a slum.

Many researchers developed similar approaches in IBM through the years but faced problems in automation i.e. the process was manually intensive. Furthermore, some challenges were present in the earlier methods, for instance, during the process of establishing correspondences in overlapping images, there were problems in matching images with illumination differences, texture differences, rotations and scale changes. However, Lowe (2004) developed an algorithm for robust matching that was invariant to scale, rotation, illumination and texture; namely the scale invariant feature transform(SIFT).

In more traditional photogrammetry, the intrinsic and extrinsic parameters of the camera had to be known for 3D modelling. However the development of structure from motion (SfM) has made it possible to use a sequence of uncalibrated, overlapping images to extract the camera motions and the 3D scenes by using detection methods such as SIFT to define and match keypoints (Snavely, Seitz, & Szeliski, 2008).

Fully automated methods for 3D model extraction using IBM were investigated in recent research work(Agarwal et al., 2010). These researchers used IBM to reconstruct the coliseum in Rome using uncalibrated photos from social sites.

Nowadays many open source and commercial software can be used to do an almost fully automatic IBM process. Joshi (2014) uses various software in creating a 3D model of a building, and then develops a method to automatically extract a 2D model from the 3D model.

IBM is a sequential process that will be discussed in this chapter for a better understanding of the entire process of creating the 3D point clouds and 2D models.

## 2.1. Image acquisition

Image acquisition is the first step carried out in an IBM process. There are several considerations when taking photos that need to be addressed. Geometric constraints such as well-distributed camera positions are important in getting the correct GPS readings and capturing the entire scene of interest. Camera position are also very important in handling occlusions. Other considerations are; well-focused images for ease and accuracy in matching homologous points, zoom level in the camera should be the same for all images (uniform focal length), high percentage of overlap for successive photos, and lastly consideration of the level of detail needed (Aerial vs terrestrial images).

## 2.2. Image Orientation

Structure from motion (SfM) is a method of recovering the 3D structure of a scene and the camera positions of a series of overlapping images. Using multiple images of a scene a sparse 3D point cloud and the camera parameters are recovered (Westoby, Brasington, Glasser, Hambrey, & Reynolds, 2012). These parameters are both intrinsic (focal length and the principal point) and extrinsic (Rotation and translation) which define the camera position in relation to the world position.

SfM uses key point detection algorithms to find matches in overlapping images. These algorithms include Scale Invariant Feature Transform (SIFT) and Speeded Up Robust Features (SURF), both of which are invariant to scale, rotation and illumination. SIFT uses difference of Gaussian images to detect keypoints and match them in corresponding images (Lowe, 2004). On the other hand, SURF uses the Hessian matrix as a keypoint detector and uses integral images to reduce the complexity of the descriptor (Bay, Tuytelaars, & Van Gool, 2006). In comparison, SIFT detects more matches than SURF but is slower in detection (Panchal, Panchal, & Shah, 2013).

SfM then implements the Random Sample Consensus (RANSAC) algorithm (Fischler & Bolles, 1981). This is an iterative method used to fit models that contain many outliers. RANSAC selects a small sample and creates a model that fits the sample. It then iteratively fits matches along the model and finally takes the model with the highest number of matches. By removing outliers, RANSAC helps in estimating the fundamental matrix.

The fundamental matrix (F) is a 3 x 3 matrix that defines the epipolar geometry of two views as shown in figure 2.1. If a point is described by  $x$  in image 1 and  $x_1$  in image 2, the two image points are related by the equation:

$$x_1^T F x = 0 \quad (2.1)$$



Once the tie points have been established, the fundamental matrix is used to compute the relative orientation of images. The matrix establishes homologous points in images.

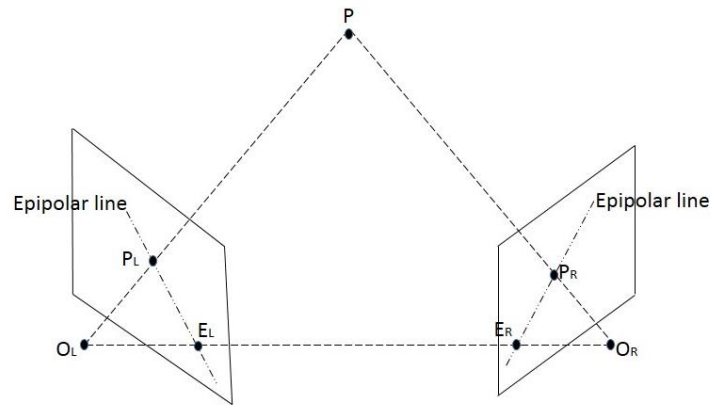


Figure 2.1: Epipolar geometry

The epipolar geometry of a stereopair means that corresponding points on both images will fall only along the corresponding image lines. Knowing the position of point A in the left image, the corresponding point in the right image will fall along the epipolar line. The fundamental matrix finds matching points in image one and constrains them along the epipolar line in image two.

SfM requires a good number of matches in the images to create the 3D structure. Triangulation or forward intersection is then done to find more matches in multiple images. The camera positions are defined in this step.

Finally, bundle block adjustment is done to refine the process. Bundle block adjustment computes the exterior and interior orientations of each image position and outputs coordinates for all points in the sparse point cloud in an arbitrary coordinate system. In summary, bundle block adjustment involves re-defining the scene geometry of the entire scene as a block (Turner, Lucieer, & Watson, 2012).

### 2.3. Point cloud reconstruction

SfM outputs a sparse point cloud and the calibrated image positions. It finds matches only in salient features. To extract more matches for object recognition, dense image matching is applied. Dense image matching involves the finding of matching points in all pixels in the images. Following improved resolution of images, the extraction of point clouds using dense matching is easily achieved (Haala, 2011).

Dense image matching can be done using optimization methods. Optimization based methods try to minimize matching costs by using the co-planarity constraint to match corresponding points between two images. Defining the disparity image using a local optimization may have limitations due to noise, occlusions and illumination.

Semi global matching (Hirschmuller, 2005) performs pixel by pixel matching and the matching costs are minimized by mutual information. It also approximates a global smoothness constraint from a combination of various 1D constraints. This method is more efficient for matching in blurred areas, poor illumination and occluded areas.

Dense image matching can also be done via patch based multi-view stereopsis (PMVS) (Furukawa & Ponce, 2010). This is an iterative method that begins with detecting matches at salient features then spreads to the neighbouring pixels. Basically, PMVS initially detects points and matches the points to all corresponding images then creates patches by triangulating 3D points from the matches. It then expands the patches using optimization functions and lastly outliers are removed by filtering.

Multi-view stereo matching methods use various algorithms. The DAISY descriptor is used for high resolution images and is suitable for large scale reconstruction of point clouds because of its efficiency in computer memory usage and rejection of outliers. The DAISY descriptor creates a dense depth map from pairs of similar epipolar lines and then uses a threshold to reject the points that are not consistently found in multiple pairs (Tola, Strecha, & Fua, 2012)

## **2.4. Reference data**

Generally the creation of point clouds using SfM does not require geotagged images or any other reference measurements, it only requires highly overlapping images. However the geoinformation in the images gives the initial camera positions that are useful in two ways:

- First, they are used in the image orientations to aid in stitching the images by detecting images that lie adjacent to each other and finding corresponding matches between them.
- Secondly, the initial camera positions are used for georeferencing the point cloud. They are used in the exterior orientation process of the images.

Ground control points (GCPs) are useful as reference measures for absolute location (georeferencing) of the point cloud. These GCPs give the point clouds real world coordinates and give the point cloud higher accuracy. They are also used in the bundle block adjustment process in improving the exterior orientation and calibration of the image positions (Shahbazi, Sohn, Théau, & Ménard, 2015).

Reference measurements of distances on the facades of buildings are useful in solving scale errors in the point cloud. This is solved by taking measurements on the physical planes, then using these measurements as scaling constraints when creating the point cloud.

## 2.5. Co-registering the point clouds

Point clouds created from images taken at different times will have different coordinate systems. This is because of the different GPS readings from the camera. These readings vary from dataset to dataset and the absolute position of the blocks cannot be determined using GPS with L1 frequency only. It is therefore necessary to register the resulting point clouds into the same coordinate system, in order to have one complete model.

Co-registration is the process of transforming two point clouds into a common coordinate system. Two point clouds are used, one is the reference (data) point cloud, while the other is the point cloud to be aligned (model). The purpose of doing this is to define the exterior orientation of the cameras of the model point cloud in the coordinate system of the reference point cloud.

Registration algorithms can be classified in two main categories (Tam et al., 2013);

- i. Rigid registration has 6 degrees of freedom (3 rotations and 3 translations) and assumes a fixed transformation between two point clouds. It is thus susceptible to noise and may require segmentation and removal of outliers. This method requires defining a few correspondences for the algorithm to work. Three corresponding points are sufficient for a rough registration.
- ii. Non-rigid registration handles changes such as stretching and deformations in the point clouds. However it requires many points to be identified in both point clouds and these may result in over fitting i.e. classifying noise as correct matches.

The most common rigid registration methods are; Principal Component Analysis (PCA), Singular Value Decomposition (SVD) and Iterative Closest Point (ICP).

### 2.5.1. Principal Component Analysis (PCA)

PCA takes two point clouds and aligns the direction of the principle axis based on the largest variance. It then performs an initial registration based on the eigenvalues of the covariance matrices. This method does not work well in noisy point clouds and is affected by outliers (Bellekens, Spruyt, & Weyn, 2014).

The rotation matrix is computed as

$$R = U_m U_d^{-1} \quad (2.2)$$

Where  $U_m$  and  $U_d$  are the eigenvectors of the model and data respectively

The translation vector is computed as

$$t = x_m - R x_d \quad (2.3)$$

Where  $x_m$  and  $x_d$  are the centres of the model and data respectively

### 2.5.2. Singular Value Decomposition (SVD)

SVD works by minimizing the Euclidean distances between corresponding points in two overlapping point clouds. Corresponding points are chosen in the two point clouds, see figure 2.2, and transformation parameters computed. One limitation is that it requires very good correspondence and is thus affected by noise.

The transformation parameters are the computed as follows (Lorsakul, 2008):

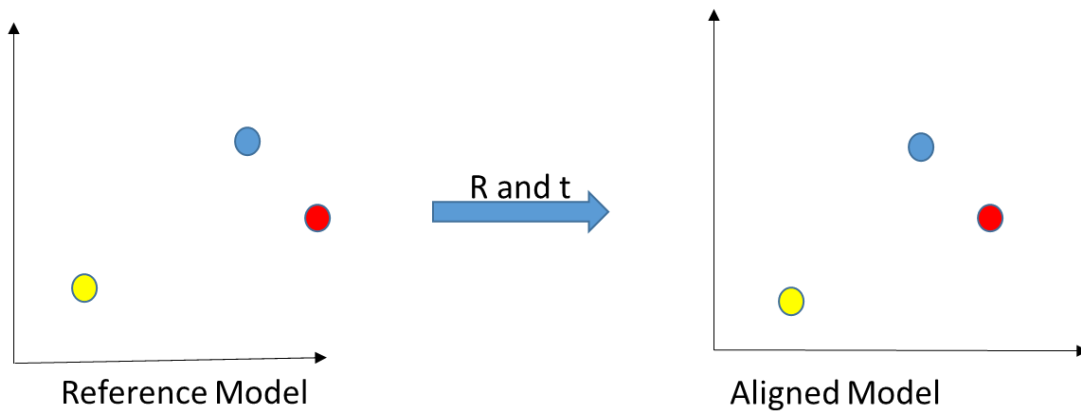


Figure 2.2: Relationship between points on two point clouds defined by rotation and translation parameters

Some points in the reference model ( $A_1, A_2, A_n$ ) are selected and their correspondences in the aligned model ( $B_1, B_2, B_n$ ) are chosen. The first step is to compute the centroids in the two point clouds i.e.  $C_a$  and  $C_b$  by simply finding the average of the vertices' coordinates.

The next step is to use SVD to compute the rotation and translation parameters

A covariance matrix ( $H$ ) is computed as:

$$H = (A_1 - C_a) * (B_1 - C_b)^T + (A_2 - C_a) * (B_2 - C_b)^T + (A_3 - C_a) * (B_3 - C_b)^T \quad (2.4)$$

Using SVD the matrix  $H$  was decomposed into 3 matrices:

$$SVD(H) = [U, S, V] \quad (2.5)$$

The rotation matrix is then computed as:

$$R = U * V \quad (2.6)$$

The translation vector would is then computed as:

$$T = C_b - R * C_a \quad (2.7)$$

### 2.5.3. Iterative Closest Point (ICP).

ICP uses an iterative approach to remove outliers from a set of data hence improving the initial approximation of the translation parameters. The initial approximation may be derived from other registration methods, In this regard, it is considered a fine registration algorithm (Bellekens et al., 2014).

This method iteratively finds the corresponding points between two point clouds using the nearest neighbour approach (Besl & McKay, 1992). The iteration continues until convergence and the rate is dependent on number of corresponding pairs. It finds the transformation parameters (R and T) by minimizing the Euclidean distance between points. These are given by equation 2.8

$$R, t = \underset{R, t}{\operatorname{argmin}} \sum_{t=1}^N \|(R p_t + t) - q_t\|^2 \quad (2.8)$$

There are two algorithms used in ICP; point to point and point to plane. Point to point is suitable for points with a higher Euclidean distance between them than the point to plane. It is slower than point to plane due to more iterations.

The basic workflow of ICP is;

- i. A set of n pairs of points are chosen between the two point clouds
- ii. A distance function is calculated as the sum of distances between the point pairs
- iii. Finally iteratively finds a rigid transform from the initialisation, that minimizes the residual distance between the point clouds

ICP is not suitable for point clouds with a small overlap. It requires good initial initialization and is sensitive to noise.



## 3. METHODOLOGY

This chapter aims to illustrate the steps taken to address the research questions in chapter one. In section 3.1, the data and study area is described. Section 3.2 describes the method of image acquisition, 3.3 describes the creation of the point cloud, and 3.4 describes the point cloud registration methods followed. Section 3.5 describes the creation of a 2D footprint. Lastly, section 3.6 and 3.7 address the accuracy analysis of the point clouds and laser device respectively.

### 3.1. Datasets

#### 3.1.1. Area of study

Two study areas were chosen for the research, one in Nairobi and the other in Enschede. For slum modelling, Mashimoni Village was chosen. This area is located approximately 1.26S, 36.86E in Nairobi's Mathare valley.

The second study area was at the University of Twente Campus located approximately 52.24N, 6.84E in Enschede. Three buildings were used to conduct some experiments. This area was chosen due to availability of reference measures such as GCPs and a map to allow for quality analysis of the point clouds. A general overview of the study areas are shown in figure 3.1 below:



Figure 3.1(a): Mashimoni village, Nairobi

Source (OpenStreetMap, 2016)

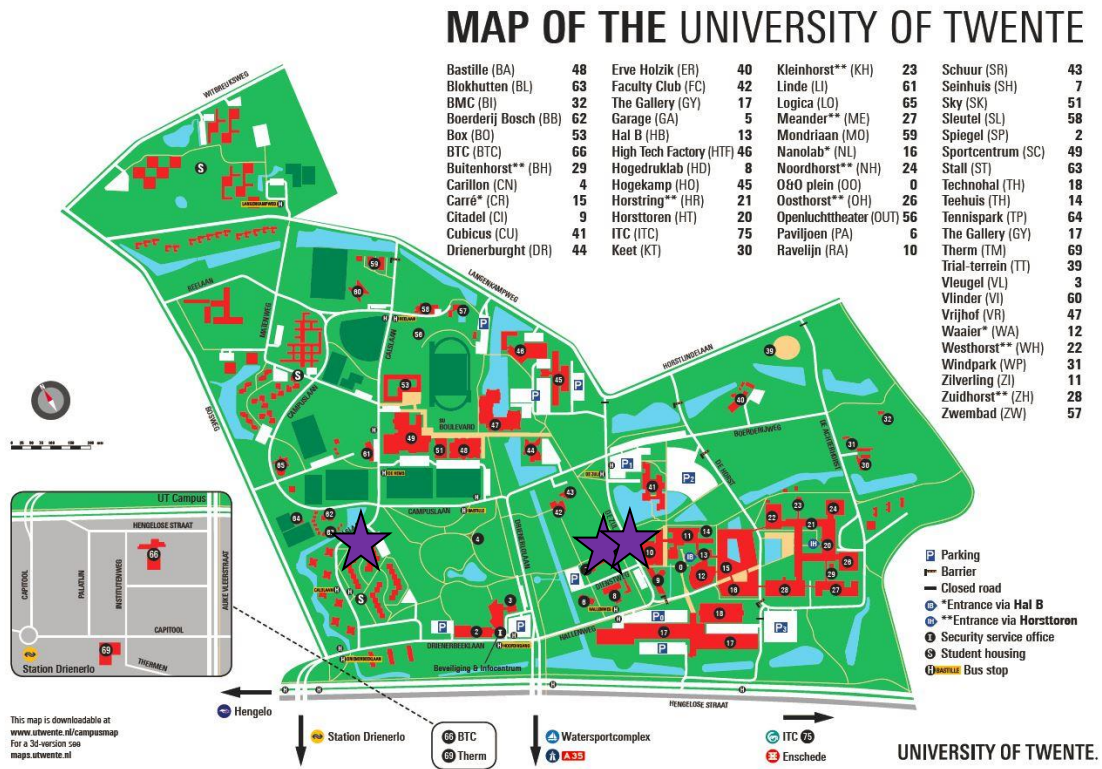


Figure 3.1(b): University of Twente campus map. Buildings mapped are marked by a purple star

### 3.1.2. Data

Geotagged terrestrial images of both the slum and buildings at the University of Twente Campus were captured using a digital camera equipped with an inbuilt L1 GPS. About 3000 images were collected in Mashimoni and 1700 at the university campus. These images were acquired with a high overlap of approximately 90%.

The specification of the camera were as follows:

**Name:** Canon Powershot S100

**Image size:** 4000x3000 pixels

**Focal length:** 5.2mm

**Pixel size:** 1.86  $\mu\text{m}$



### 3.1.3. Equipment

Table 3.1: Software and Hardware

	Software and Hardware	Uses
1	Pix4D	Creation of 3D point clouds and 2D footprint
2	Cloud Compare	Quality assessment of 3D point clouds/Registration of point clouds
3	R studio/ SPSS	Statistical analysis of the 2D and point clouds
4	Matlab/ C++	Scripting and programming
5	ArcGIS	GIS applications
6	Global Mapper	Point cloud visualisation and GIS applications
7	Digital Camera / iPad	Image acquisition
8	Ike Spike device	Reference measurements
9	100m Measuring tape	Reference measurements
10	Geodetic GPS	Acquisition of reference data

#### 3.1.3.1. Ike Spike Laser Device

The Spike laser-measuring device (IkeGPS, 2015), shown in fig 3.2, was used to take reference measurements of some building facades that would be used to scale the model. It was used as a substitute to a measuring tape due to its advantages such as; it can be used by a single operator, it is fast and quick to record measurements.



Figure 3.2: Spike laser device mounted on an iPad®

Spike consists of a laser range finder and 3D compass. Once it is attached to a smart phone, it pairs to the GPS and camera of the smartphone via Bluetooth. The laser range finder uses the time of flight principle (figure 3.3) to calculate the distance to the target.

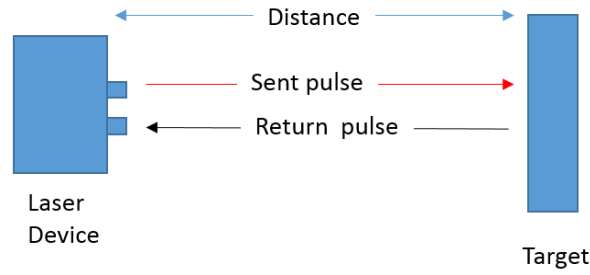


Figure 3.3: Time of flight principle

By sending a laser pulse to the object, it computes the time taken for the laser to return and thus calculates the distance (d) given as:

$$d = \frac{1}{2} ct \quad (3.1)$$

Where c is the speed of light and t is the time of travel

Measurements of planar heights, lengths and widths can be done from the images. A point x, on the real world plane is mirrored as x' on the image. Using 2D homography (projective planar transformation) the relationship between image plane and world plane are defined as

$$x' = Hx \quad (3.2)$$

Where H is a non-singular 3x3 matrix with 8 degrees of freedom

Once a plane is defined on the image it relates to the real world plane using four coplanar points and thus the lines on the real world plane(L) can be defined on the image plane(l) by equation 3.3(Zeng, Zhang, Mu, & Wang, 2013)

$$L = H^T l \quad (3.3)$$

Using the distance (d) from the image to the plane and the angle between the camera centre and the plane, measurements can be done on the image that reflect the real world plane measurements. A sample measurement is shown in figure 3.4.



Figure 3.4: Sample measurement made using spike laser device

### 3.2. Image acquisition

A series of terrestrial images were acquired in Mashimoni village. Image acquisition required proper planning and the challenge was how to capture high resolution, high overlapping photos. Factors considered to develop an optimal approach in the acquisition of the images were: coverage of the entire area of interest, level of detail required, image overlap from multiple views, same zoom level for all images, best GPS observations, reference measurements, minimal occlusions in the images, camera position with respect to the building structures and optimizing the field of view.

Considering the characteristics of the area of interest the methodology used had to be different from the conventional approaches used in close range photogrammetry. In the narrow corridors, a *step and shoot* approach was used, as shown in figure 3.5, whereby the operator shot images as he walked along the corridors. Landscape oriented photos were taken capturing both the right and left facades as well as the ground.

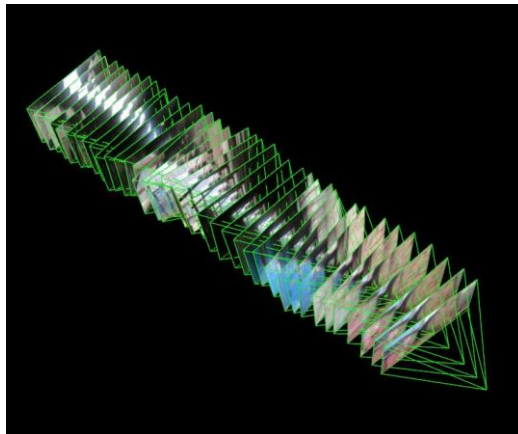


Figure 3.5: Image acquisition along corridors

The images were taken with a high percentage overlap to ensure good coverage of the area. Images were taken over several days due to the considerable size of the slum and the durability of the battery of the camera.

At the boundaries of the slum, the standard approach for terrestrial photogrammetry was used. Images were taken progressively in succession from one camera position to the next. This ensured a high overlap of up to 90%. The same method was used at the UT for image acquisition. This was done for three buildings. The data at the university would be used for quality assessment of the point clouds and 2D model. Image acquisition technique around the buildings is illustrated in figure 3.6.

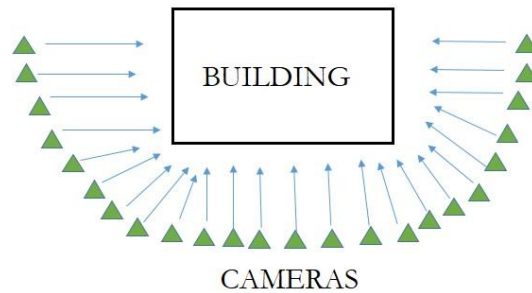


Figure 3.6: Image acquisition method of buildings at University campus

Reference data was acquired in both areas of study. Some measurements were taken using the Spike laser device and measuring tape. Some more reference data was taken at the UT using a RTK GPS. Lastly, an orthophoto of the slum was provided by Pamoja Trust, a Nairobi based NGO.

### 3.3. Creating a Point cloud

An IBM approach was used to create a 3D point cloud of the scene and a 3D mesh. The steps involved included structure from motion and dense image matching. The principles of SfM and dense image matching are explained in chapter 2.

SfM was used to perform image orientation in the images and create a sparse 3D point cloud. This was done using the Pix4D software (Pix4Dmapper, 2015). Reference measurements were used to scale and georeference the point cloud in the SfM process.

After SfM was done, dense image matching was used to find more homologous points in multiple images. The process was also done in Pix4D. The result of this process was a dense 3D point cloud. Colour was added to the 3D point clouds for object recognition and surface representation. The point clouds were then be exported as .las or .xyz format.

### 3.4. Co-registration of the point clouds

Processing of the data was done day by day or in some cases, object by object. In this case, a lot of manual editing and creation of tie points is required to co-register the different point clouds together. To overcome this problem, a rigid (6DoF) transformation was used to determine the geometric relationship between the overlapping point clouds i.e. the transformation parameters between two point clouds as shown in figure 3.7.

The main objective of the co-registration was to define new exterior orientation (EO) parameters of the cameras of model point cloud in the coordinate system of the reference point cloud. After the transformation parameters are defined, these EO parameters can be defined.

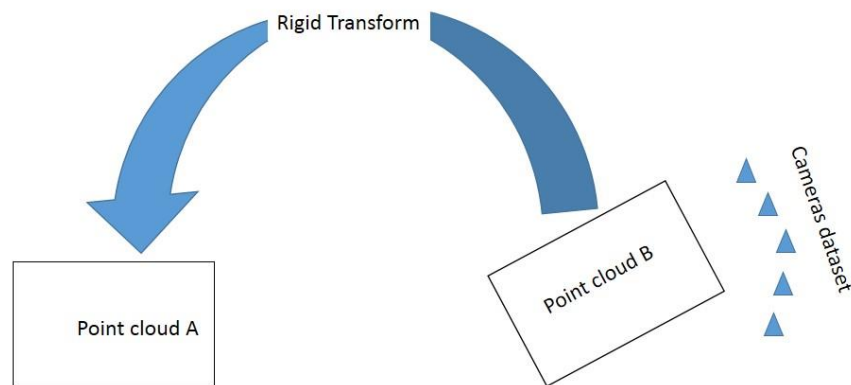


Figure 3.7: Co-registration of point cloud.

#### 3.4.1. Basic steps of the registration workflow

1. Two adjacent point clouds were loaded in Cloud compare (Girardeau-Montaut, 2015) and at least 3 corresponding points at the overlap were selected. From figure 3.7, point cloud A is used as the reference model while point cloud B is the model to be aligned.
2. A point to point alignment was done by searching for matches in the overlap area, then transformation of point cloud B into the coordinate system of the reference model (point cloud A).
3. The rotation matrix and translation vectors between the two models were derived.

4. Using the rotation matrix and translation vectors, the initial camera positions were transformed using a Matlab script. The new camera positions  $(x', y', z')$  were computed by the rotation and translation matrix from the initial camera  $(x, y, z)$  positions as:

$$\begin{bmatrix} x' \\ y' \\ z' \\ 1 \end{bmatrix} = \begin{bmatrix} a & b & c & tx \\ d & e & f & ty \\ g & h & i & tz \\ 0 & 0 & 0 & 1 \end{bmatrix} \begin{bmatrix} x \\ y \\ z \\ 1 \end{bmatrix}$$

New exterior orientations of the cameras of the aligned point cloud were obtained.

5. Lastly, the images of the two models were imported into Pix4D and the initial camera positions of the aligned were replaced by the newly computed camera positions. The weights of the horizontal and vertical accuracy were set to a custom lower value and used to reprocess the models. This is shown in figure 3.8.

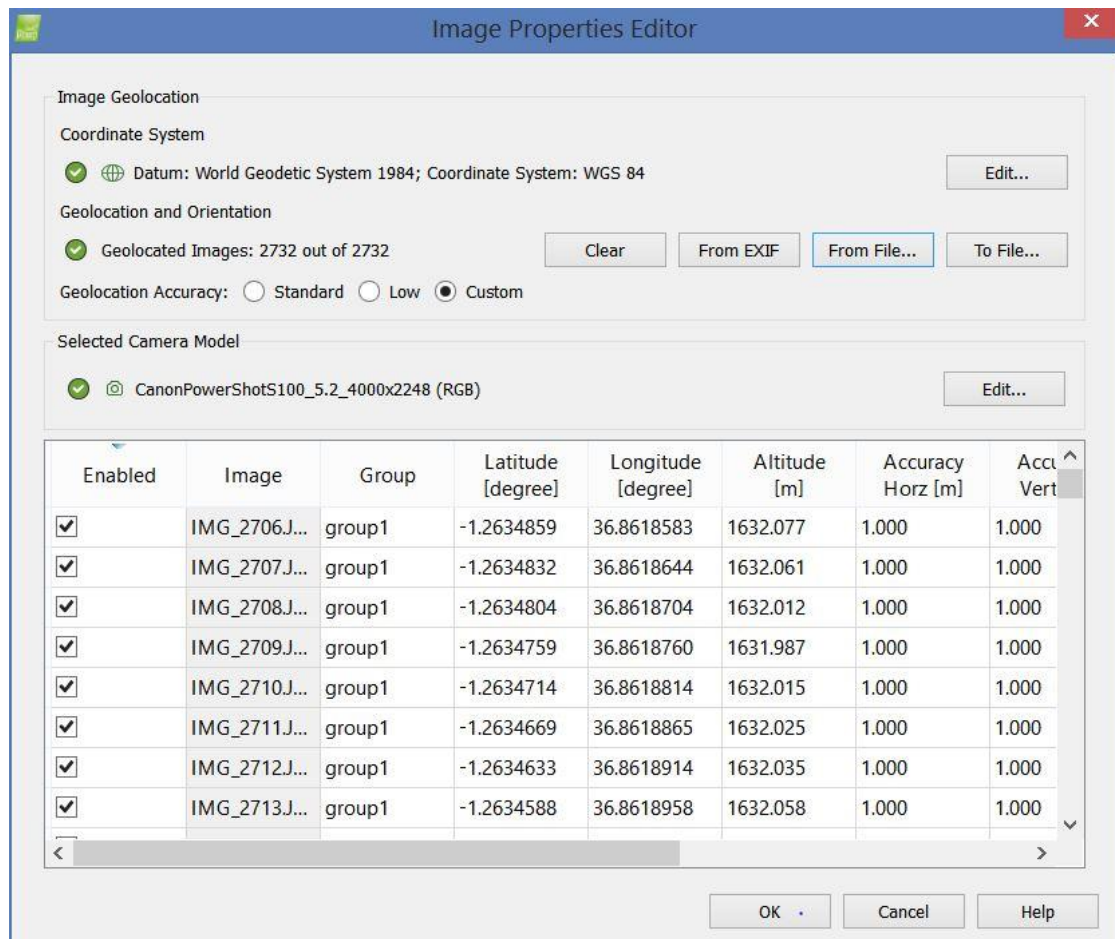


Figure 3.8: Image properties in Pix4D

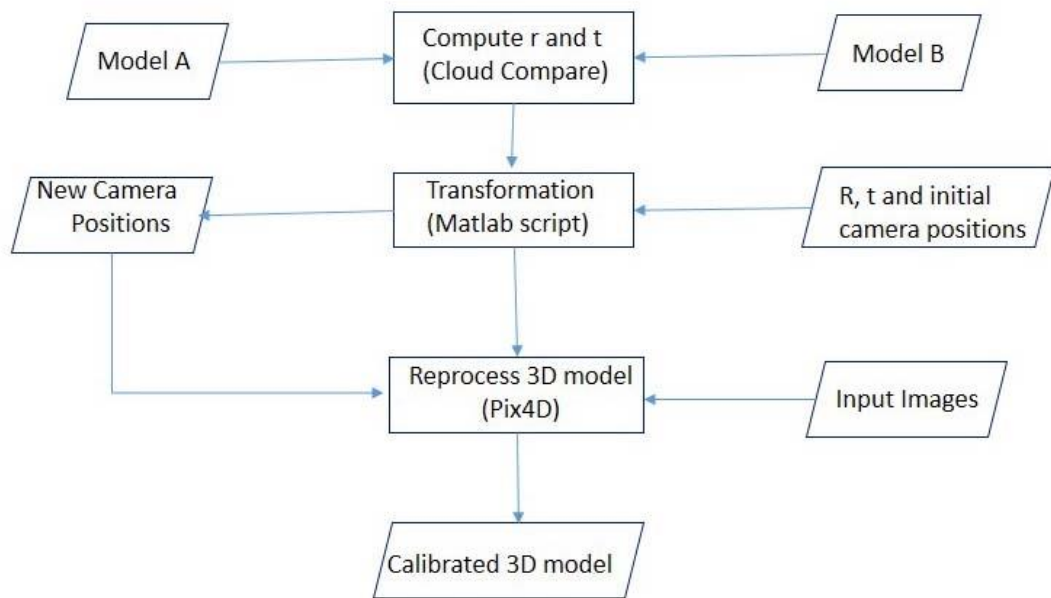


Figure 3.9: Registration of point clouds workflow.

### 3.5. Creation of a 2D outline

Feature extraction was done in this stage. This involved extracting the 2D footprint of features from the 3D point cloud. It was very difficult to define horizontal and vertical planes in this environment due to occlusions in the data, gaps, clutter and fuzzy footprints between the ground and building facades. Automatic extraction of the outline was not possible and manual methods of creating the 2D model were applied.

This was done by creating polylines at the intersection of the vertical (wall) and horizontal (ground) planes in the point cloud. The vertices of the polylines were then refined in the multi view images by selecting corresponding points in the overlapping images as illustrated in figure 3.10. The polylines were exported as ESRI shapefiles and were merged into one 2D model. The product was a 2D outline in a CAD or shapefile format that can be used in a cadastral application.



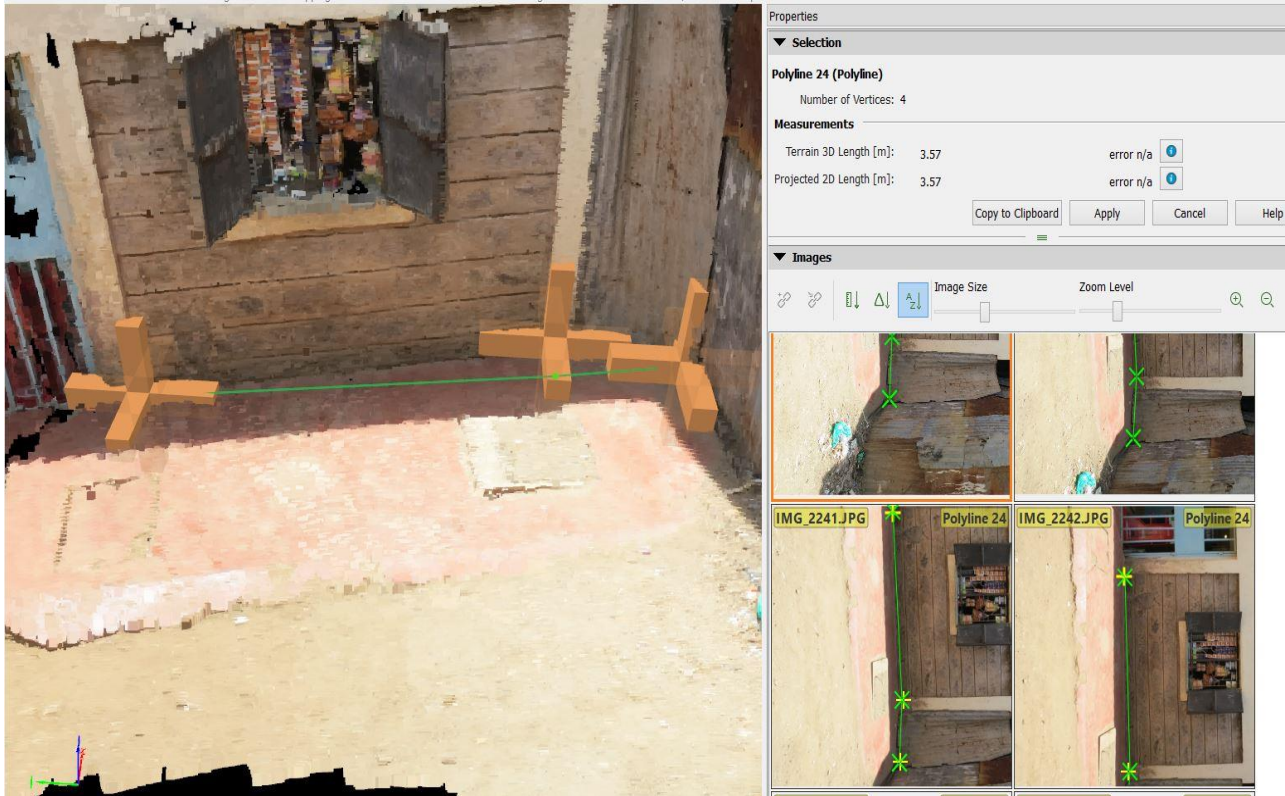


Figure 3.10: 2D extraction from the 3D model and refinement in the overlapping images

### 3.6. Quality assessment of 2D and point clouds

In the 3D point cloud, some problems were imminent because of errors from the instrument e.g. poor GPS readings. Other sources of errors included poor illumination, clutter and the surface properties of the objects. These resulted in poor geolocation affecting the matching in SfM, point cloud noise, poor point density and gaps in the data. Occlusions were because of the characteristics of slums e.g. narrow corridors, cluttered scenes. Initial quality checks could be done just by visualization of the 3D point cloud and errors such as gaps could be identified.

Using software such as Cloud Compare, internal accuracy assessment was done by plane fitting while external accuracy assessment was done using reference data.

Statistical analysis was done on the models to check for systematic and random errors. To analyse the quality of the camera's internal GPS (for georeferencing of the model), measurements were done at the University of Twente Campus using geodetic RTK GPS and used as reference data.

Furthermore, orthophotos from the Nairobi data were used to check the quality of the 3D and 2D models.



### **3.7. Quality analysis of Spike laser measurement device.**

The device was used in scaling the 3D point cloud, thus, it was essential to check its relative accuracy, quality and limitations in the research. Measurements using Ike Spike were taken of a block of buildings and other planar surfaces at the University of Twente Campus.

Different set ups and views were used to perform a systematic analysis on different surfaces such as brick walls, wood, metallic surfaces and glass surfaces. Different angular measurements and scales were taken in multiple images to different surfaces. They were later compared to reference data from measurements done with a measuring tape.

In addition, existing topographic and cadastral data was used for further analysis. Assessment was done by analysing the results from the Spike laser with these reference data. More accuracy assessment was done in Nairobi by taking additional measurements using a measuring tape.

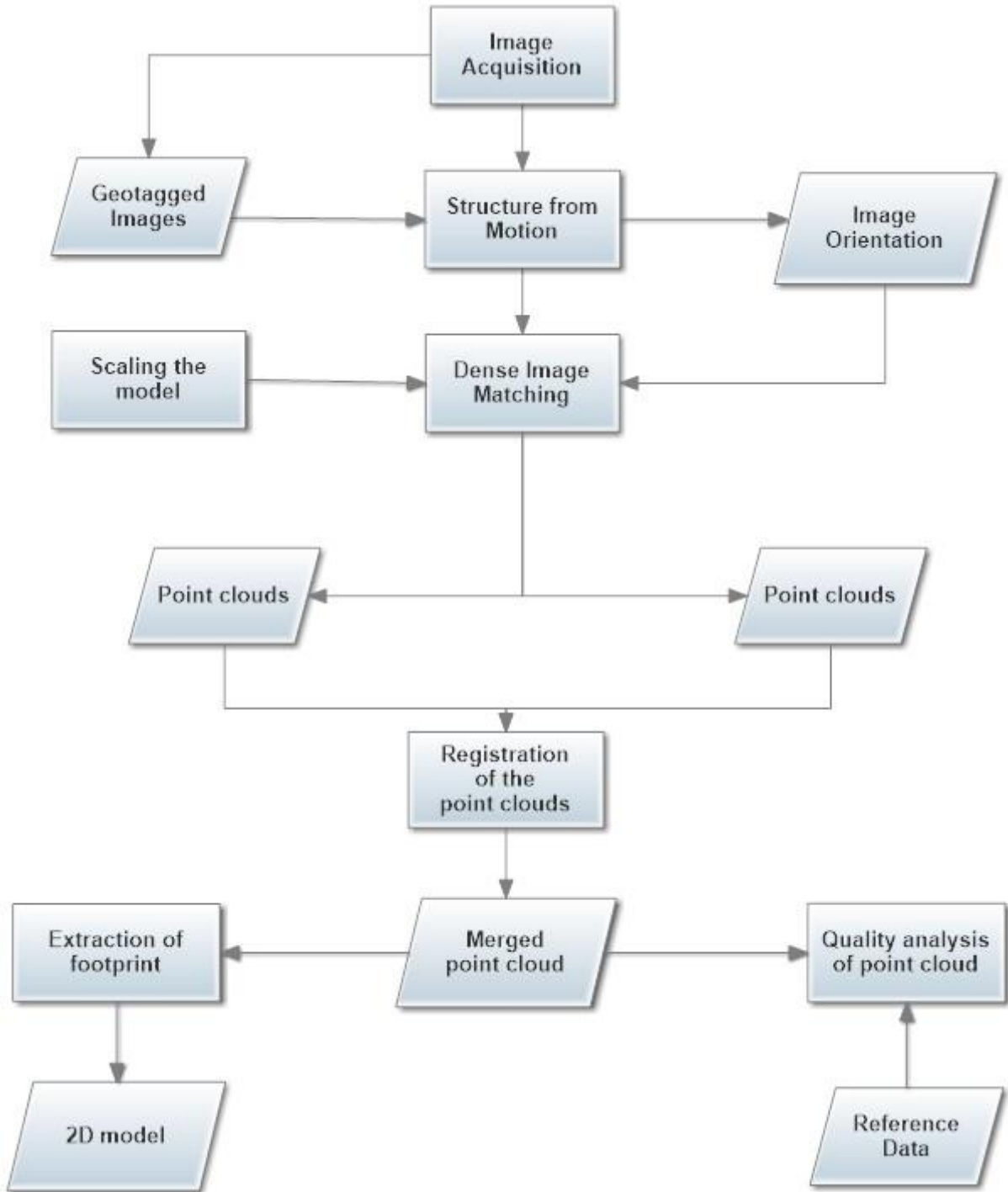




Figure 3.11: Proposed methodology workflow

**Symbology**

	<i>input or output</i>
	<i>process</i>

## 4. RESULTS AND DISCUSSIONS

### 4.1. Creation of point clouds

Using structure from motion and dense image matching point clouds were created for both areas of study and the quality assessment was done using reference data as explained in chapter 3.

#### 4.1.1. University of Twente models

Three buildings at the University of Twente were chosen for the quality analysis of the models and laser measurements. 1713 images were taken and several reference measurements done using RTK GPS and spike laser. 3D point clouds and 2D models were created and the quality assessment was done. A sample point cloud is shown below in figure 4.1

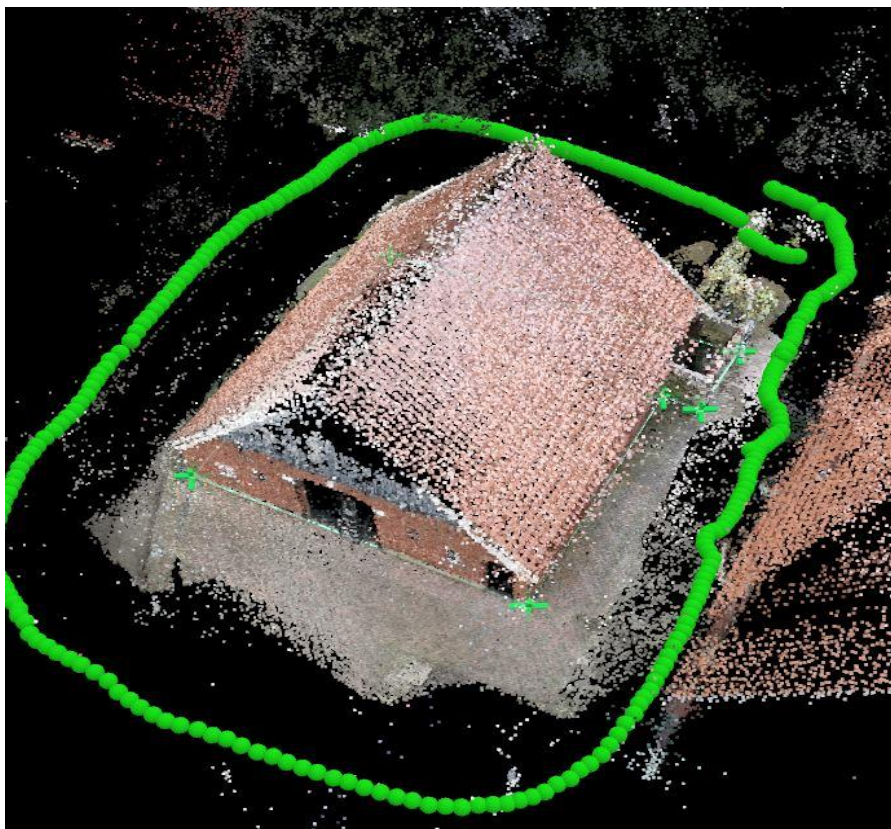


Figure 4.1: Point cloud including camera positions

**Experiment 1: Faculty Building**

Three models were created for this building:

- i. Point cloud containing RTK GPS information: This was created using geoinformation from the camera and 3DGCPs measured by RTK GPS.
- ii. Point cloud created from Camera information only: This was created solely from geoinformation from the camera only i.e. L1 GPS. It included scaling constraints from the spike laser.
- iii. Point cloud with 2D GCPs from campus map: This was created using geoinformation from the camera, including 2DGCPs extracted from a cadastral map of the campus.

The point cloud with RTK GPS information was used as the reference model. The corner points of the buildings were measured in the three datasets and accuracy analysis done.

Table 4.1: Building corner points using RTK GPS compared to L1 GPS

Point cloud with RTK GPS				Point cloud with L1 GPS only				Residuals GPS			Euclidean Distance
Name	X	Y	Z	Name	X	Y	Z	dx	dy	dz	D
GPS1	439.375	39.306	29.645	PC1	439.661	40.756	30.709	-0.286	-1.450	-1.064	1.477
GPS2	440.409	27.953	29.396	PC2	440.714	29.269	30.767	-0.305	-1.316	-1.371	1.350
GPS3	441.850	53.308	29.353	PC3	442.074	54.720	30.246	-0.224	-1.412	-0.893	1.429
GPS4	442.258	38.599	29.180	PC4	442.760	40.078	30.286	-0.502	-1.479	-1.106	1.561
GPS5	447.721	20.539	29.515	PC5	448.158	21.916	31.113	-0.437	-1.377	-1.598	1.444
GPS6	448.902	26.466	29.462	PC6	449.010	27.666	31.064	-0.108	-1.200	-1.602	1.205
GPS7	452.894	18.084	29.500	PC7	453.474	19.623	31.280	-0.580	-1.539	-1.780	1.645
GPS8	453.254	19.582	29.510	PC8	453.830	20.907	31.349	-0.576	-1.325	-1.839	1.445
GPS9	454.894	42.085	29.218	PC9	455.278	43.530	30.572	-0.384	-1.445	-1.354	1.495
GPS10	455.755	17.744	29.262	PC10	456.240	19.075	31.145	-0.485	-1.331	-1.883	1.416
GPS11	456.173	20.286	29.246	PC11	456.759	21.704	31.009	-0.586	-1.418	-1.430	1.534
GPS12	456.543	50.532	29.398	PC12	456.673	52.013	30.676	-0.130	-1.481	-1.611	1.487
GPS13	461.020	40.601	29.085	PC13	461.234	42.323	30.706	-0.214	-1.722	-1.621	1.735
GPS14	461.482	44.076	29.215	PC14	461.755	45.546	30.707	-0.273	-1.470	-1.492	1.495
GPS15	465.330	18.704	29.394	PC15	465.823	20.207	31.453	-0.493	-1.503	-2.059	1.582
GPS16	466.366	24.236	29.257	PC16	466.787	25.781	31.235	-0.421	-1.545	-1.978	1.601
GPS17	468.028	23.850	29.418	PC17	468.493	25.393	31.455	-0.465	-1.543	-2.037	1.612
GPS18	471.377	42.052	29.534	PC18	471.609	43.687	31.369	-0.232	-1.635	-1.835	1.651

Table 4.2: Residual errors of model point cloud

	X	Y	Z
RMSE	0.402	1.460	1.620
TOTAL ERROR(XY-axis)	1.514		
MEAN ERROR	-0.372	-1.455	-1.586
STANDARD DEVIATION	0.155	0.123	0.339

The RMSE from the selected corner points show an RMSE error of 0.402, 1.460 and 1.620 on the x, y and z axes respectively. This means that the positional accuracy of the point cloud is within the expected accuracy of L1 GPS. The standard deviation values show that the observations have smaller errors in X and Y but are bigger in the Z axis. Looking at the residuals of the different axes, there is a larger error in the Y axis as compared to the X axis. This shows there is a bias in the Y axis and the residuals are independent in the individual directions.

The total error in the Euclidean distance is 1.514 which is within the theoretical accuracy of GPS with L1 frequency only. The histogram of the Euclidean distance shown in figure 4.2, shows normality in the distribution with some outliers. This shows that the value of the residual (i.e. Euclidean distance) between the reference and model is random.

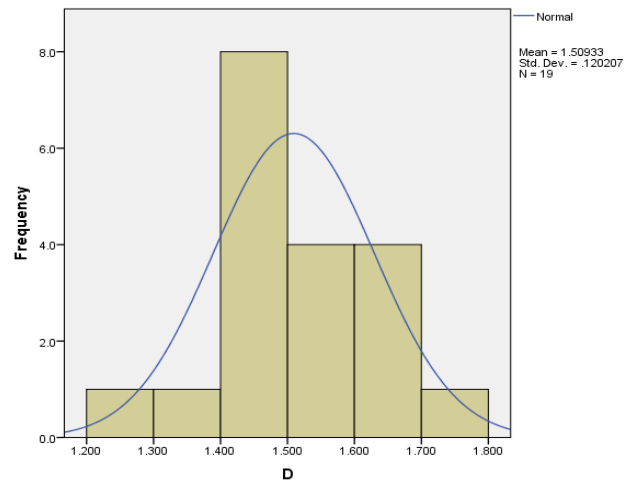


Figure 4.2: Histogram of the Euclidean distance

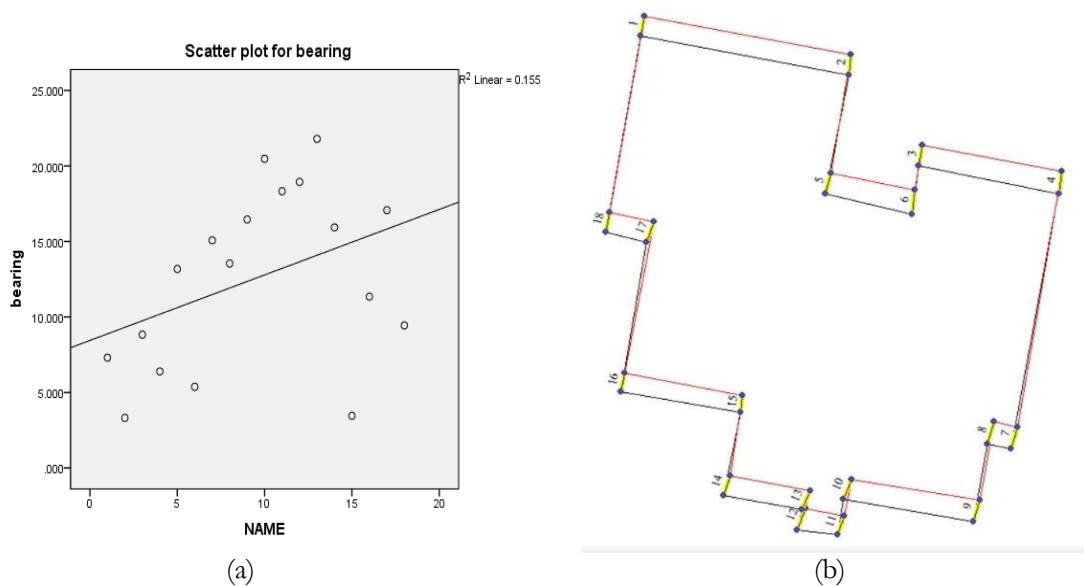


Figure 4.3: (a) Scatter plot for bearing and (b) bearing of model points from the reference points derived from the RTK GPS point cloud: Both show random errors.

The scatter point of the bearing (Figure 4.3a) is derived from the position of the corner points of the L1 GPS model with respect to the reference (RTK GPS) model. It shows random errors which are mainly attributed to projection errors from 3D to 2D. This is also evident in the 2D outline, shown in figure 4.3b, that there is a bias in the Y axis. This shows a systematic error in the dataset.

The area and perimeter measured from the 2D outline created from the 3 sets of point clouds shows some differences that are attributed to the scaling errors in 3D to 2D projection.

Table 4.3: Comparison of area and perimeter

	<b>Area</b>	<b>Perimeter</b>	
Point Cloud with 3DGCPs	730.71	133.78	
Point Cloud with 2DGCPs	726.12	132.8	
Point Cloud with L1	734.79	133.18	
<b>Difference Area (sq.m)</b>		<b>Difference Perimeter(m)</b>	
3DGCPs - 2DGCPs	3DGCPs - L1	3DGCPs - 2DGCPs	3DGCPs - L1
4.59	-4.08	0.98	0.6

The RMSE from the selected corner points from the point cloud corrected with 2D GCPs show an RMSE of 0.120 and 0.095 in the X and Y axis respectively. The total error on the XY axis was 0.153m. The positional accuracy was good as shown in figure 4.4 below, the two models almost overlay perfectly on each other. The subtle differences can be mainly attributed to digitizing and projection errors. It was concluded that the 2D GCPs can be used to georeference the model accurately in the absence of 3D GCPs.

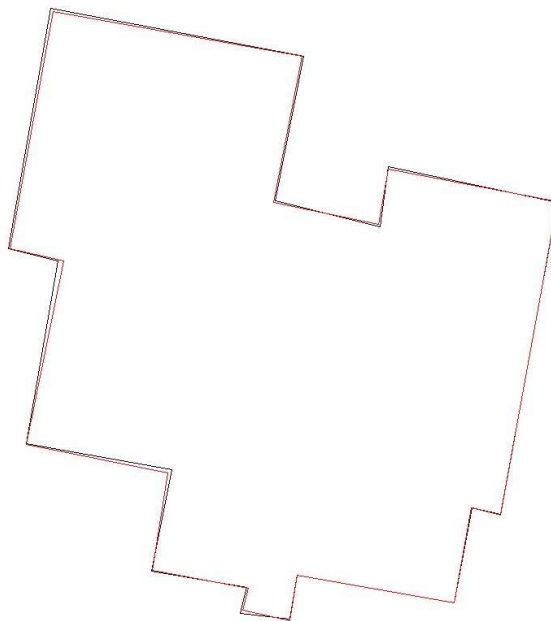


Figure 4.4: Comparison of point cloud corrected with 2D GCPs (in black) with one corrected with 3D GCPs from RTK GPS (in red)

**Experiment 2: Store**

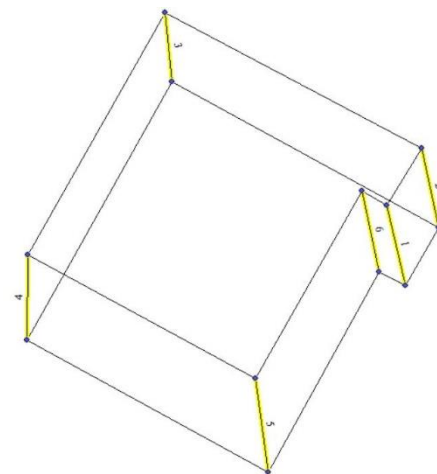
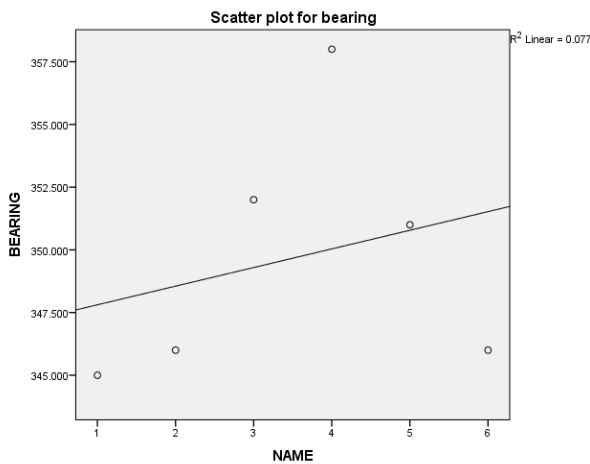
Analysis was done on 3 point clouds derived similar to experiment 1 above. In this dataset, the residuals in the Y axis was larger contributing to an increased total error in the Euclidean distance. There was a visible skew, shown in figure 4.5(b), in the 2D outline due to projection errors. The difference in the area and perimeter between the derived 2D outline was larger, showing scaling errors.

Table 4.4: Building corner points using RTK GPS compared to L1 GPS

Name	X	Y	Z	Name	X	Y	Z	dx	dy	dz	D
GPS1	977.401	311.389	27.811	PC1	977.529	314.732	26.868	-0.129	-3.343	0.943	3.345
GPS2	983.307	321.586	27.276	PC2	983.021	324.384	26.675	0.285	-2.798	0.601	2.812
GPS3	987.116	306.046	27.866	PC3	986.634	309.809	28.494	0.481	-3.763	-0.628	3.794
GPS4	991.563	314.053	28.081	PC4	990.866	317.273	27.349	0.697	-3.220	0.732	3.294
GPS5	992.612	313.513	27.905	PC5	991.876	316.716	27.418	0.736	-3.203	0.486	3.286
GPS6	993.951	315.822	27.941	PC6	993.269	318.980	27.191	0.682	-3.158	0.750	3.231

Table 4.5: Comparison of area and perimeter

	Area	Perimeter	
Point Cloud with 3DGCPs	47.931	132.66	
Point Cloud with 2DGCPs	48.571	135.69	
Point Cloud with L1	45.438	118.55	
<b>Difference Area (sq.m)</b>		<b>Difference Perimeter(m)</b>	
3DGCPs - 2DGCPs	3DGCPs - L1	3DGCPs - 2DGCPs	3DGCPs - L1
-0.64	2.493	-3.03	14.11



(a)

(b)

Figure 4.5: (a) Scatter plot for bearing and (b) bearing of model points from the reference points: Both show random errors.

**GCP distribution**

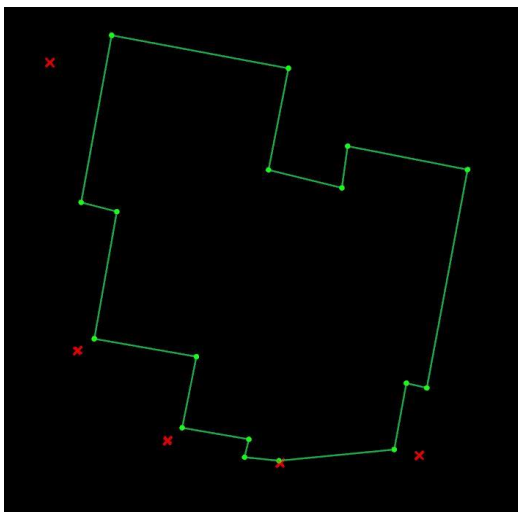
Ground control points were set up around the two buildings and were used in the point cloud referencing. Table 4.6 shows the residuals of the 3D GCPs computed as the difference in the reference GCP and the measured GCPs in the images. The projection errors were smaller in GCPs which were verified/ marked in more images. In experiment 1 the GCP residuals had a higher RMS error in the Y and Z axis than in experiment 2. This was due to the poor distribution of GCPs in the block as shown in figure 4.6.

Table 4.6a: Accuracy of GCPs (Experiment 1)

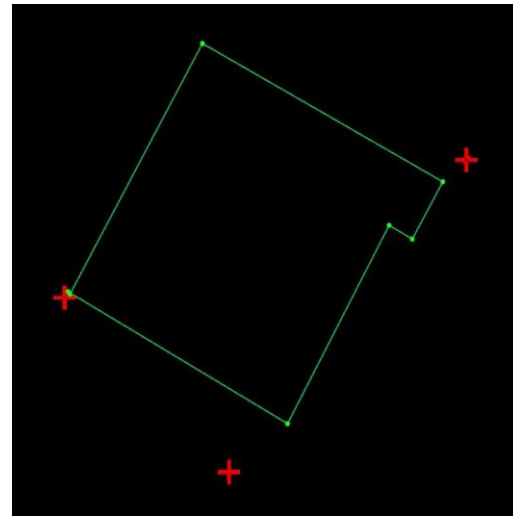
GCP Name	Error X [m]	Error Y [m]	Error Z [m]
BL12	-0.009	-0.002	-0.006
BL11	0.006	0.002	0.023
BL10	0.022	0.037	0.006
BL09	-0.024	-0.06	-0.049
BL08	0.008	0.015	0.029
RMS Error [m]	0.0158	0.0325	0.0278

Table 4.6b: Accuracy of GCPs (Experiment 2)

GCP Name	Error X [m]	Error Y [m]	Error Z [m]
BL06	-0.022	-0.021	-0.008
BL04	0.021	-0.012	0.001
BL02	-0.005	0.021	-0.002
Mean [m]	-0.0020	-0.0039	-0.0029
RMSE[m]	0.0179	0.0184	0.0046



(a)



(b)

Figure 4.6: Distribution of GCPs (shown as red crosses) in two buildings (a) Experiment 1 (b) Experiment 2



#### 4.1.2. Mashimoni Dataset

About 3000 images were taken in Mashimoni slum (Nairobi). They were collected over several days and point clouds were reconstructed for individual days and objects.



Figure 4.7: Sample point clouds

Six individual point clouds were created. Table 4.7 shows some results from the quality report.

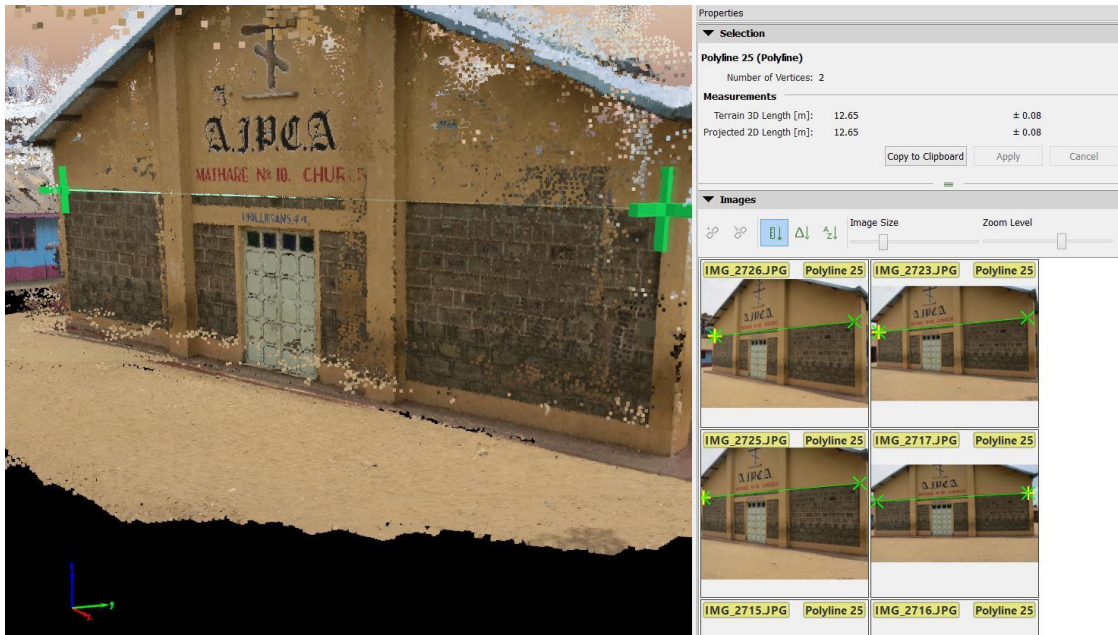
Table 4.6: Descriptions of datasets

	<b>Calibrated Images</b>	<b>GSD</b>	<b>Number of Blocks</b>
Dataset1	992/992	0.17cm	1
Dataset2	498/537	0.14cm	2
Dataset3	679/757	0.11cm	6
Dataset4	677/677	0.18cm	1
Dataset5	341/341	0.12cm	1
Dataset6	373/373	0.11cm	2

In some datasets, multiple blocks were created, this was due to insufficient matches in the images caused by cluttered scenes, occlusions and gaps between images. The matching was in some cases solved by introducing manual tie points. Some of the images were not calibrated due to insufficient key-point matches between corresponding images.

#### 4.1.2.1. Accuracy assessment of the point cloud

A few measurements were taken on the ground and the same measured in the images for computing the relative accuracy. This is illustrated in figure 4.8.



(a)



(b)

Figure 4.8: (a) Measurements done on the point cloud and refined in the multiview images (b) reference measurements done using the physical facade

**Using Reference measures on the physical façade**

	Façade	Images	Error
Measurement 1	12.68	12.65	0.03
Measurement 2	3.26	3.19	0.07

Taking the first measurement we compute the residual error as the difference between the distance measured on the physical façade (D1) and the one measured in the point cloud (D2). We can then compute the relative error using the formula:

$$\frac{E}{D1} \times 100 \quad (4.1)$$

The relative error is **0.47%**

Taking the second measurement, the theoretical / expected error is 0.47% of 3.26 which is equal to 0.015m. Therefore, theoretical measured distance on image should be 3.26 – 0.015 which is equal to 3.25m. However, the actual measured distance on image is 3.19m. The difference between the theoretical distance and measured distance is 0.06m therefore the dataset is within the expected accuracy.

The relative ratio between the two measurements should be the same if there are no distortions in the block.

$$D_1 / D_2 \approx D_3 / D_4 \quad \text{we get } 1.002 \approx 1.022$$

The two ratios are almost identical and it can be concluded that the error is a scale error. The error should be approximately the same in the whole data set. The introduction of GCPs can solve this error.

### Using reference measures from Orthophoto

From the orthophoto, more measurements were done and used as reference measures as shown in figure 4.9 below. Corresponding measurements were done on the merged point cloud and the relative errors computed.

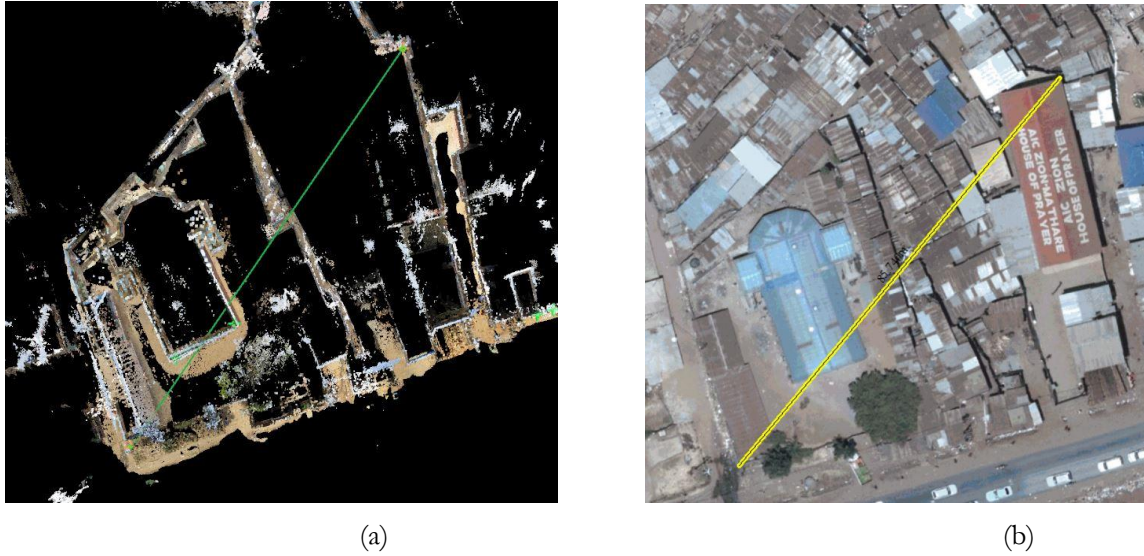


Figure 4.9: (a) Measurements done on the point cloud (b) Corresponding measurement done on the orthophoto

Table 4.7: Comparison of measurements on orthophoto and merged point cloud

	Orthophoto	Point cloud (MP)	Relative errors %	Expected error	Theoretical measurement on point cloud (TP)	Difference (MP- TP)
M1(Reference)	57.28	57.51	0.401			
M2	85.74	86.21	-0.548	0.343	86.08	0.126
M3	85.87	86.59	-0.838	0.344	86.21	0.375
M4	163.32	164.75	-0.875	0.654	163.97	0.775
M5	115.74	116.18	-0.380	0.464	116.20	-0.024
M6	158.68	161.27	-1.632	0.636	159.31	1.953

Taking the first measurement we compute the error as the difference between the distance measured on the orthophoto and the one measured in the point cloud. Using equation 4.1, we calculate the relative errors of all measurements.

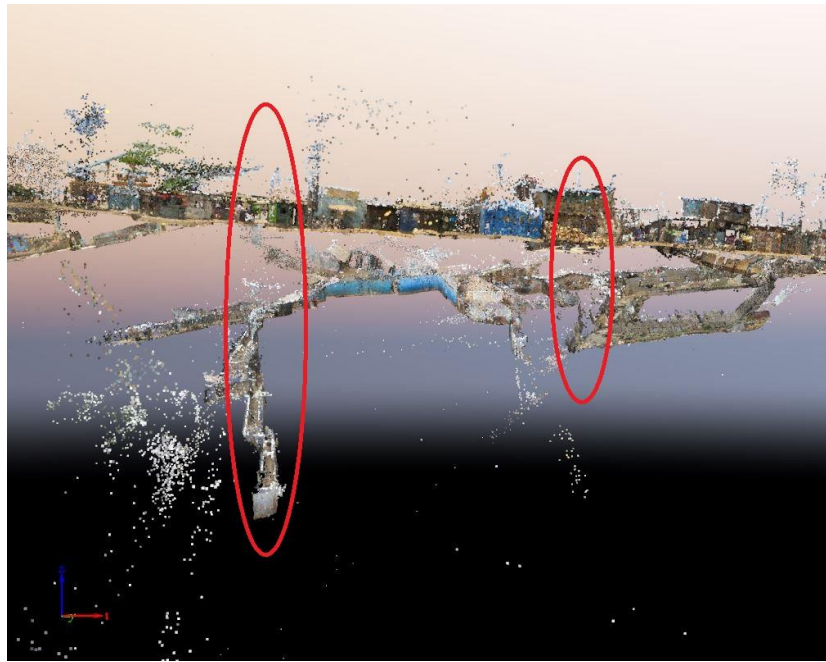
Taking more measurements we compute the theoretical errors for all, using measurement 1 as the reference. Looking at table 4.7 above, it was observed that the errors in the dataset were random and were caused by scale errors within the point cloud. There were some distortions on the merged point cloud.

More analysis using the orthophoto is done in chapter 4.4.

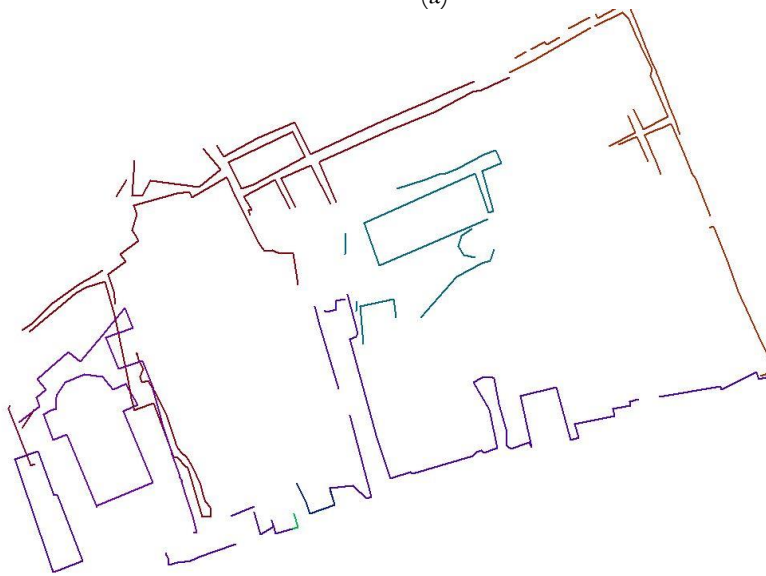


## 4.2. Automatic registration of point clouds

As explained in chapter 2 and 3, registration differences were expected. Merging the point clouds into one model was a challenge. Registration errors were encountered as shown in the figure 4.10.



(a)



(b)

Figure 4.10: (a) Registration errors shown on the point cloud (b) Registration errors shown on the 2D model

#### 4.2.1. Registration using corresponding points (Rough registration)

Cloud compare was used in the registration of the point clouds. To register two point clouds point picking alignment was first done. The first step involved manual segmentation of the point clouds so as to remain with the overlap area only (figure 4.11). After this was done, corresponding point pairs were input and alignment done as shown in figure 4.12. The transformation matrix was output in the console. This would be used in the next ICP registration.

This method worked well in the overlapping area as shown in figure 4.13, but there was some skew and orientation errors further away from the overlap area. Further away from the overlap area the point cloud was tilted and there were huge errors in the z-axis. The elevation differences in the point clouds were large.

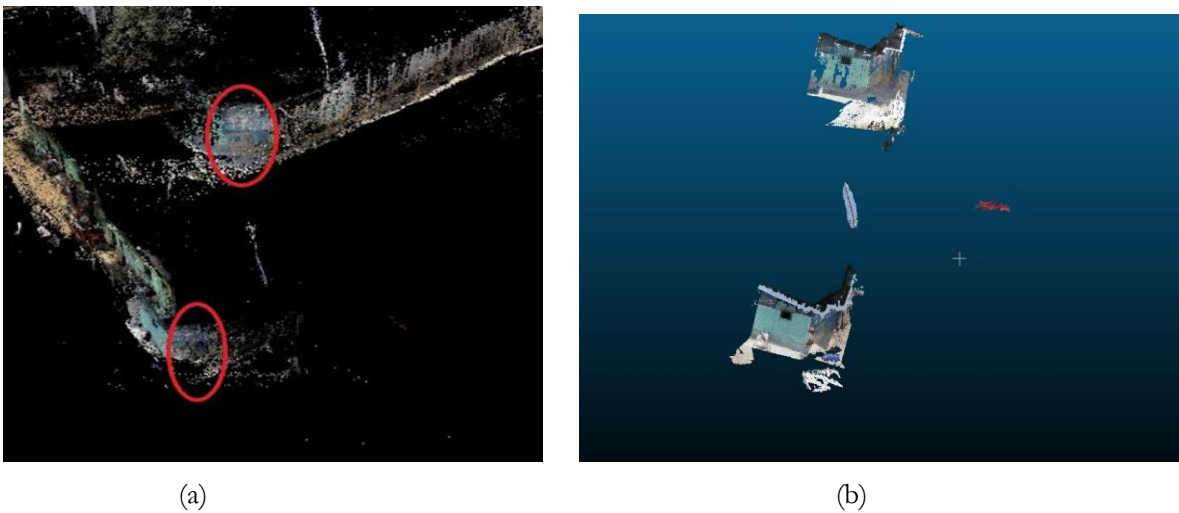


Figure 4.11: (a) Overlapping area between two point clouds showing the registration differences (b) Segmented area of the overlap

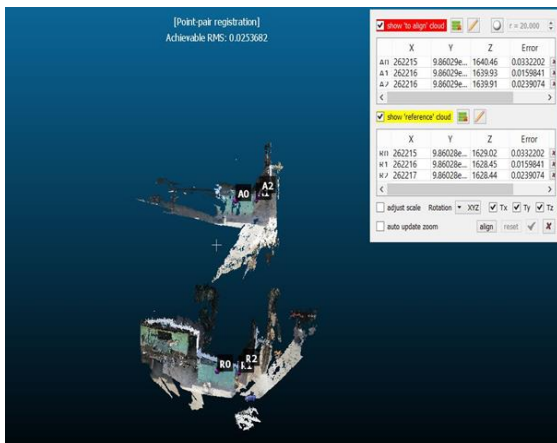


Figure 4.12: Corresponding points of the point clouds using point picking (rough registration)

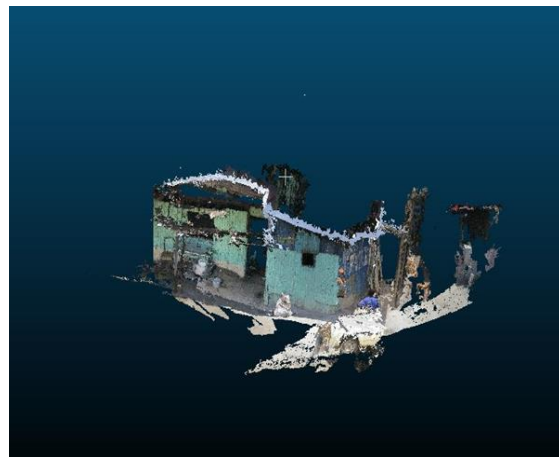


Figure 4.13: Aligned overlap area

#### 4.2.2. Registration using ICP

After doing the rough registration, it was necessary to apply fine registration. This was done using the ICP algorithm explained in chapter 2.5.3. The segmentation of the point cloud done in 4.2.1 above was necessary because ICP only matches points that represent the same surfaces. Including the non-overlapping area will result in poor registration. After ICP was done a transformation matrix was output.

After getting the transformation parameters, new camera positions were computed using a Matlab script. This was done for all the overlapping pairs of point clouds. These new camera positions were input in Pix4D as the new initial positions and processing was done for the entire data. After the processing was done a new point cloud of the entire area was created.

Visual checks were done to the point cloud and it was noted that registration errors were still present. The calibrated camera positions were checked and it was noted that they were still erroneous especially in the z-axis.

A rigid registration method was used, which is sensitive to outliers and limited overlaps thus the registration was problematic further away from the overlap area.

#### 4.2.3. Correction of model using 2D control points from the orthophoto.

After registration using the rigid registration, the orthophoto was used to further correct the model. Several points were picked in the orthophoto (figure 4.14) and used in the SfM process as 2D GCPs while others were used as check points. The idea was to select corresponding points especially in the problematic areas.



Figure 4.14: Corresponding points in orthophoto and point cloud

Reprocessing was done using the 2D GCPs as reference data. This method improved the registration in some parts of the model by aligning corresponding points and correcting the elevation error. The elevation error still remained a problem as shown in figure 4.15.

The main challenge was identifying matching points from the orthophoto and point cloud. Some points were identified on roofs on the orthophoto but their corresponding points could not be identified in the point cloud, as it lacked roof information.

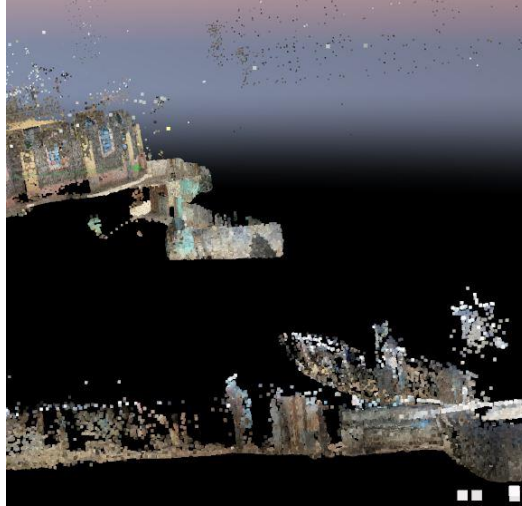


Figure 4.15: Elevation differences still persisted after the correction using 2DGCPs

#### 4.2.4. Correction of heights using digital elevation model

After doing the registration using the transformation parameters and the 2D GCPs, registration in the horizontal plane was good. However, there was still an error in the elevations. The point clouds registered well in overlapping areas but there was a rotation in the z axis shown by the calibrated camera positions in fig 4.16

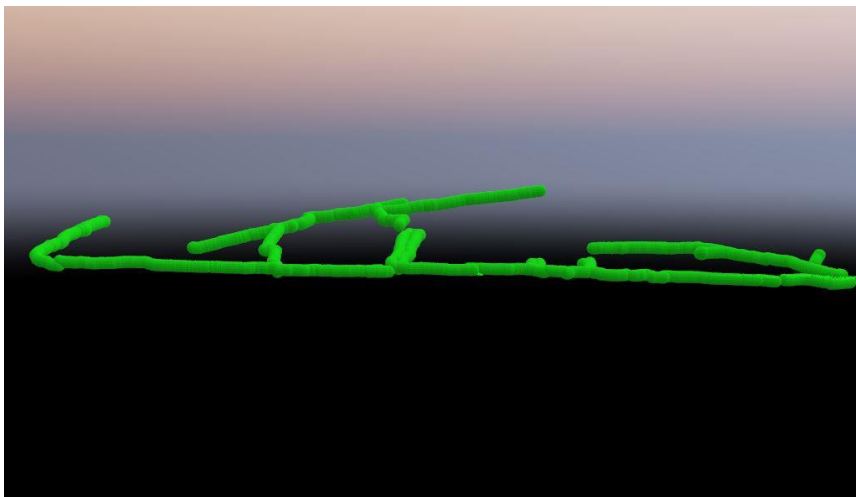


Figure 4.16: Camera positions with the elevation errors



To correct the elevation error, a digital elevation model (SRTM 3 arc second/ 90m resolution) was introduced. Considering that the area is a small relatively flat area without major changes in gradient, the resolution of the DEM was good enough for the corrections.

The camera positions were overlaid on the DEM and new heights were extrapolated from the DEM onto the image positions. The new image positions were input in Pix4D and used to reprocess the point cloud. The elevation problem was fixed as can be seen in figure 4.17 and 4.18.

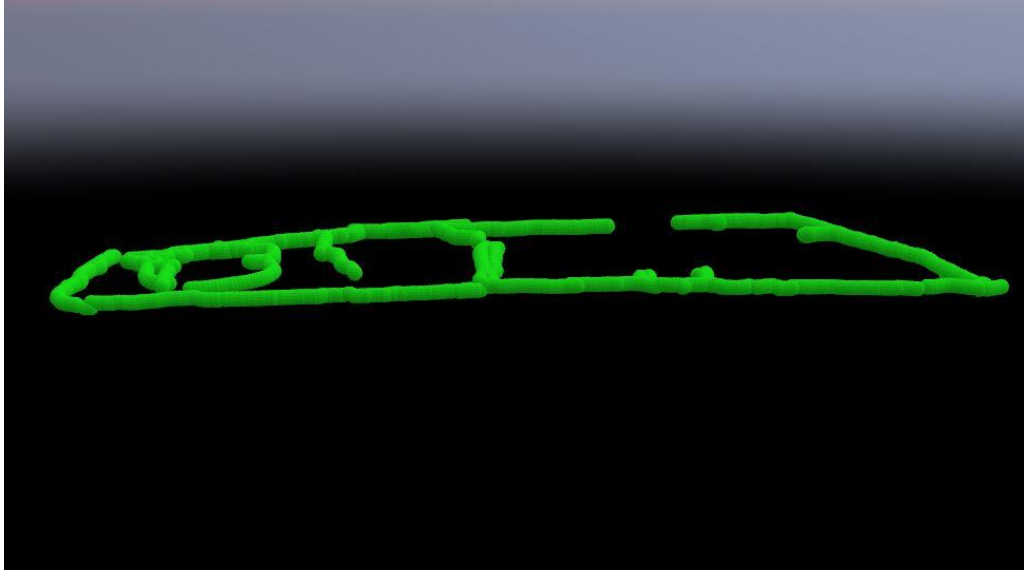


Figure 4.17: Camera positions corrected for height using elevation model

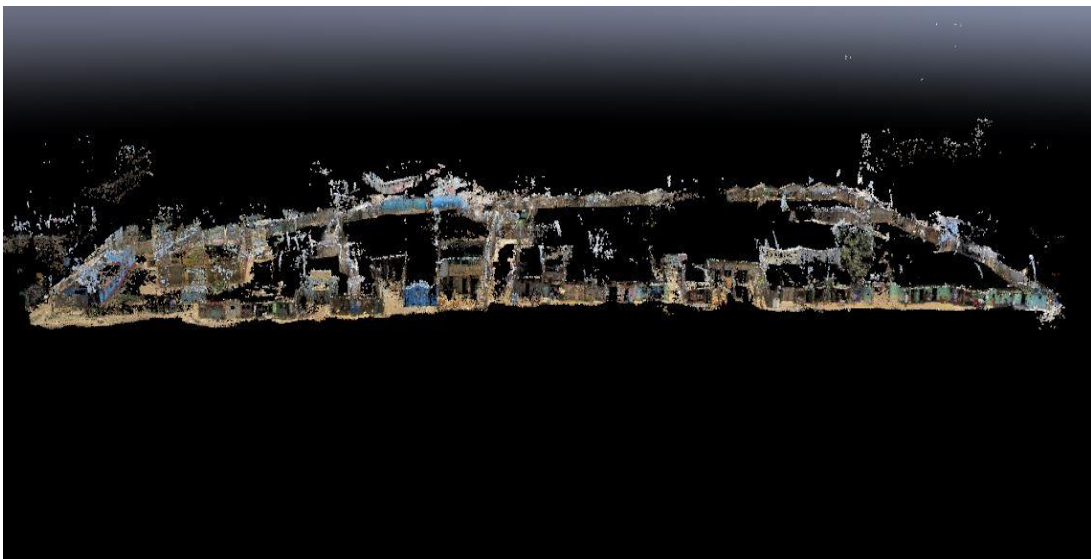


Figure 4.18: Full point cloud of study area; co-registered and merged.

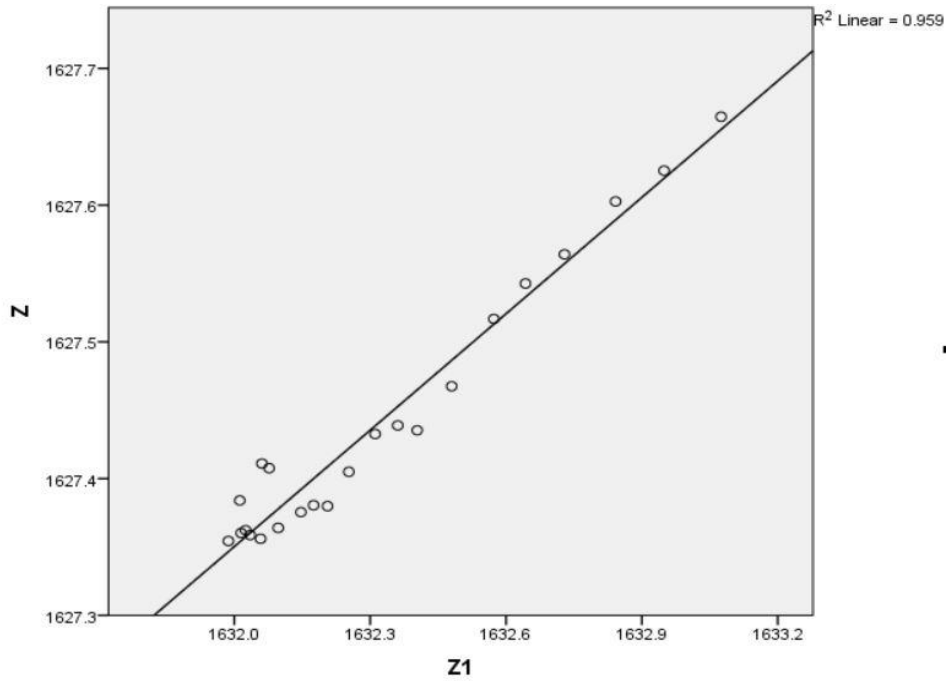


Figure 4.19: Scatter plot of initial elevation against computed elevation from DEM

The scatter plot, in figure 4.19 above, shows a positive correlation between the heights extrapolated from the DEM and those from the initial camera positions from the L1 GPS. This implies that the initial error in the heights was a systematic error from the L1 GPS.

### 4.3. Visualization of the point cloud

The densified point cloud was exported as a laser file format (las) for visualization and manipulation in 3D modelling and GIS software. Figure 4.18 shows the final registered and corrected point cloud. The same was rendered as a video (mp4 format) solely for the purpose of visualization. The video animation was also uploaded on YouTube with the following link:

[https://www.youtube.com/watch?v=5nhNIUZ\\_V3I&feature=youtu.be](https://www.youtube.com/watch?v=5nhNIUZ_V3I&feature=youtu.be)

#### 4.4. 2D footprint of the slum

A 2D outline of the slum was extracted from the registered point cloud and refinement in the multi-view images. This was later exported in shapefile format. There were some gaps in the model due to gaps and occlusions in the point cloud. This is shown in figure 4.20



Figure 4.20: 2D outline of the slum overlaid on orthophoto

Some points were selected on both the 2D model and the orthophoto, which was used as the reference model, and some comparison was done.

Table 4.8: Comparison of corresponding points in point cloud and orthophoto

Name	X	Y	Name	X	Y	Residuals_X	Residuals_Y	D
ch1	77.852	284.777	mtp196	72.408	282.625	5.445	2.152	5.855
ch2	81.845	261.652	mtp193	79.517	261.319	2.328	0.333	2.352
ch3	69.206	257.121	mtp192	67.097	255.228	2.109	1.893	2.834
ch4	58.807	277.976	mtp204	54.139	274.766	4.668	3.210	5.665
cp1	49.758	277.169	mtp171	46.835	273.807	2.922	3.362	4.455
bld1	57.867	269.804	mtp3	54.679	266.382	3.188	3.422	4.677
cp2	210.455	283.646	mtp209	208.556	281.408	1.899	2.238	2.935
cp3	181.203	363.988	mtp2	181.376	363.764	-0.173	0.224	0.283

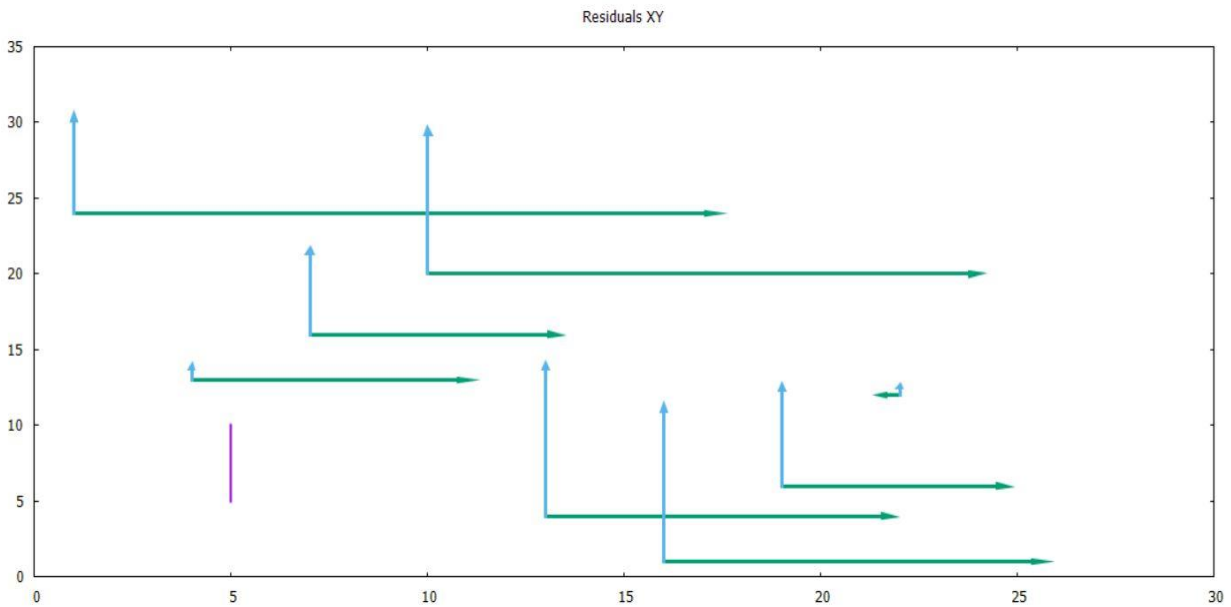


Figure 4.21: Error vectors for x and y axes

The mean error in the xy axis was 3.6m. According to the expected accuracy of L1 GPS, these results were good. The error vectors in figure 4.21, show that there are random errors in both directions. Scaling errors and distortions in the block are mainly the reason for this.

The metadata of the orthophoto is

The flying height (H) =1372m

Focal length (f) = 100mm

Scale = f/H = 1:7300

Size of the sensor unit (Sw) =7.5 mm

Image width (Iw) = 50056 pixels

$$\text{GSD} = \frac{Sw \cdot H \cdot 100}{f \cdot Iw} \quad (4.2)$$

$$\text{GSD} = 0.206\text{cm}$$

Table 4.9: Geolocation errors from 2D checkpoints

	X	Y	Z
Sigma [m]	2.332	1.194	0.139
RMS Error [m]	2.943	1.287	0.640

From the GSD we can compute the theoretical standard horizontal error of orthophoto as  $2 \times \text{GSD} = 0.41$  for the normal case. Looking at the errors from the 2D checkpoints in the point cloud (table 4.9), we can conclude that the error in the horizontal plane is approximately 5 times the theoretical error.



#### 4.5. Spike laser measuring device accuracy analysis

The spike laser device was used to take some measurements on some surfaces. This was done on a brick wall, wooden surface and a metallic surface. On the brick wall measurements were done on three facades. The measurements on the image plane are affected by the rotation angles and the distance between target and object. Therefore some experiments were done using different angles and distances. Some statistical analysis was then carried out as follows.

##### *Façade 1*



Figure 4.22: Measurement of brick wall

Taking the reference measurement from the tape i.e. 4.74, the residuals were calculated as:

$$\text{Residuals} = \text{observed} - \text{measured}$$

Table 4.10: Residuals of Spike measurements

Distance to target	Bearing to target	Measured distance on plane	Residuals
16	139.2	4.74	0
16.18	142.6	4.75	-0.01
16.03	142.4	4.73	0.01
16.06	144.1	4.72	0.02
16.27	147.5	4.69	0.05
16.5	145.1	4.64	0.1
16.77	144.5	4.65	0.09
17.09	142.1	4.67	0.07
14.7	159.3	4.72	0.02
14.13	164.5	4.64	0.1

Distance to target	Bearing to target	Measured distance on plane	Residuals
13.6	142.7	4.67	0.07
13.24	147	4.72	0.02
13.2	145.6	4.76	-0.02
13.17	145.9	4.75	-0.01
13.12	140.5	4.77	-0.03
13.41	141.9	4.77	-0.03
12.18	139	4.81	-0.07
11.55	133.5	4.79	-0.05
8.87	129.1	4.72	0.02
8.69	134.8	4.84	-0.1
7.8	139.5	4.73	0.01

Some descriptive statistics were done on these residuals and are as follows:

Mean	<b>0.012</b>
Standard Error	<b>0.012</b>
Standard Deviation	<b>0.054</b>
Sample Variance	<b>0.003</b>
Confidence Level (95.0%)	<b>0.025</b>

The residuals observed are within millimetre level and this shows precision in the measurements. The standard deviation shows that the measurements have little variation between them and have high precision

### Correlation

There were two variables that affect the observations namely;

1. Distance to the target and
2. Bearing (angle) of observation.

	<i>Bearing</i>	<i>Measured</i>		<i>Distance</i>	<i>Measured</i>
Bearing	1		Distance	1	
Measured	<b>-0.509</b>	1	Measured	<b>-0.540</b>	1

The correlation coefficient shows that the variables are not correlated and are independent from each other.

### Regression analysis using target distance

SUMMARY OUTPUT	
<i>Regression Statistics</i>	
Multiple R	0.539
R Square	0.291
Adjusted R Square	0.254
Standard Error	0.046
Observations	21

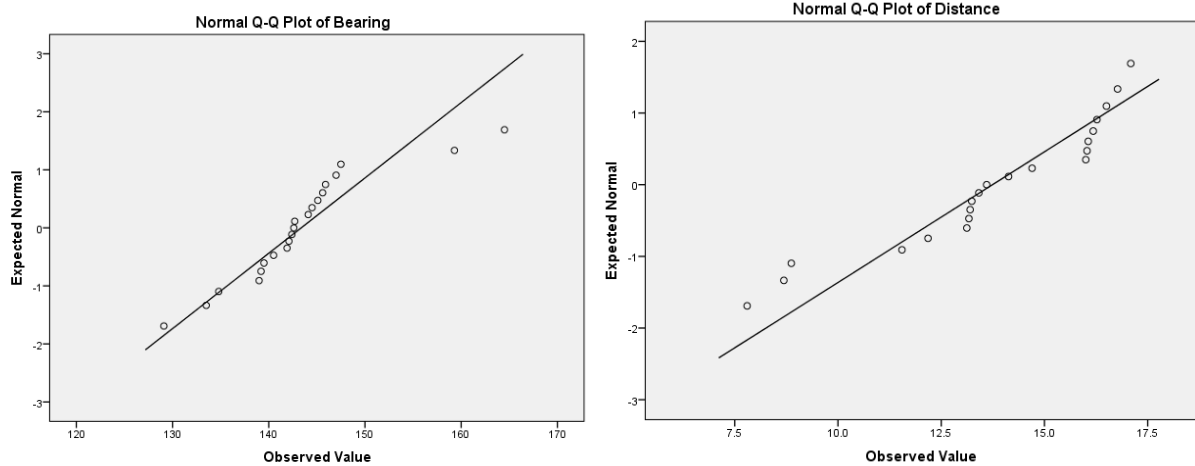
**Model**  $Y = a + bx$   
 $Y = 4.874326 + -0.01068x$

Measured	Predicted	Residuals Msd - Pred
4.74	4.70	0.04
4.75	4.70	0.05
4.73	4.70	0.03
4.72	4.70	0.02
4.69	4.70	-0.01
4.64	4.70	-0.06
4.65	4.70	-0.05
4.67	4.69	-0.02
4.72	4.72	0.00
4.64	4.72	-0.08

Measured	Predicted	Residuals Msd - Pred
4.76	4.73	0.03
4.75	4.73	0.02
4.77	4.73	0.04
4.77	4.73	0.04
4.81	4.74	0.07
4.79	4.75	0.04
4.72	4.78	-0.06
4.84	4.78	0.06
4.73	4.79	-0.06

The RMSE was 0.044 showing only a small error in the observed measurements.

**Normality of the variables**



(a) (b)

Figure 4.23: Normal Q-Q plots of (a) bearing (b) distance to target

Tests of Normality						
	Kolmogorov-Smirnov <sup>a</sup>			Shapiro-Wilk		
	Statistic	df	Sig.	Statistic	df	Sig.
Bearing	.201	21	.027	.891	21	.023

Tests of Normality						
	Kolmogorov-Smirnov <sup>a</sup>			Shapiro-Wilk		
	Statistic	df	Sig.	Statistic	df	Sig.
Distance	.176	21	.089	.893	21	.026

The Q-Q plots (figure 4.23) show that the datasets are from a common normal distribution. The Shapiro-Wilk tests of normality and the plots above shows a normal distribution of the variable and thus we can predict that the model will work at all the observed distance and angles.

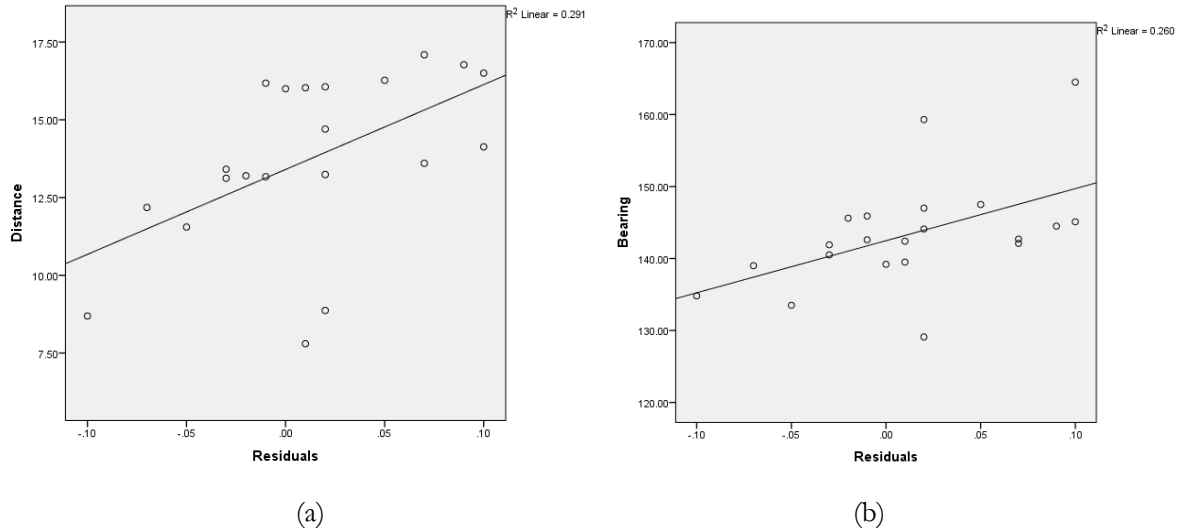


Figure 4.24: Scatter plots of (a) distance vs residuals (b) bearing vs residuals

From the observations, the two variables, distance and bearing (angle) were independent of the measured data. There were no systematic errors in the measurements. The graphs and plots above showed random errors in the dataset.

The differences in the measurements were due to the operator's skill in defining the plane surface, using manual alignment in the image while doing measurements. If the alignment is done accurately, the measurements are almost identical regardless of the distance and bearing.

To analyse the effect of various surfaces such as reflective properties of a surface, more analysis of the spike measurements were done on different surfaces. These were done on a wooden surface, smooth metallic surface and on a glass surface. These surface measurements are shown in appendix 3.



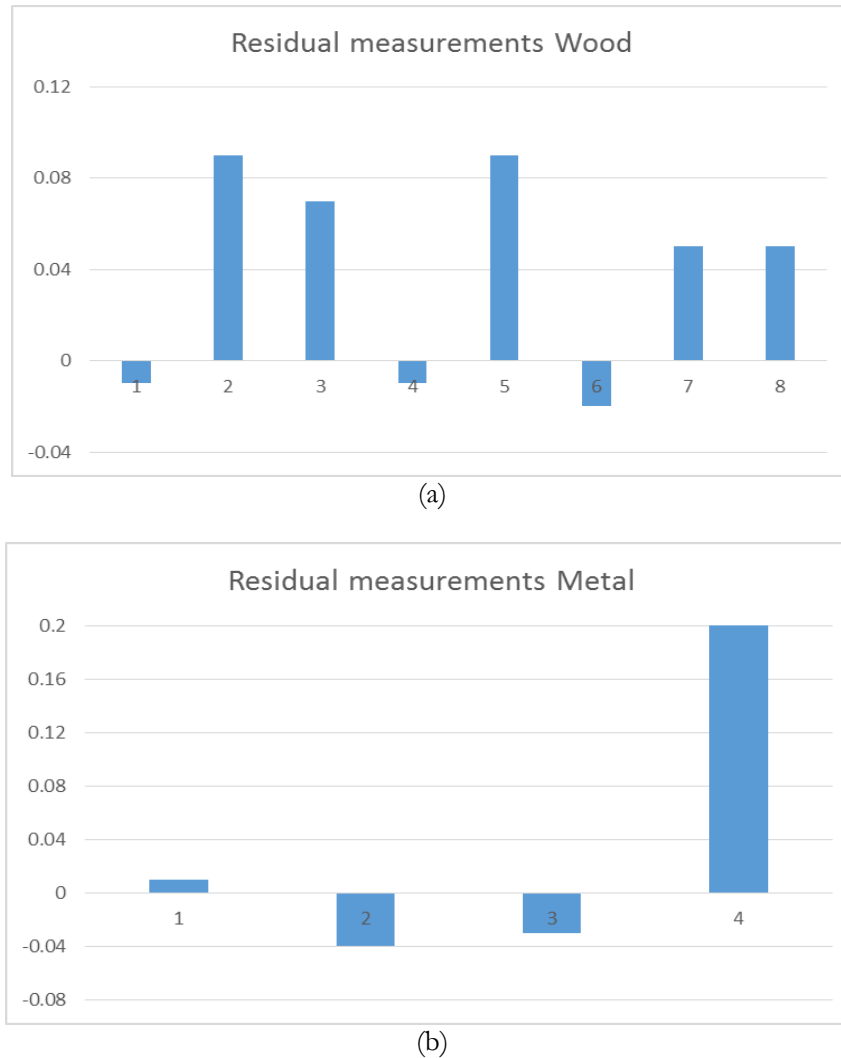


Figure 4.25: Histograms showing residuals of (a) wooden surface (b) metallic surface

The residuals on the wooden and metallic surfaces showed good precision in the results and thus it was concluded that the laser device works well on both surfaces.

However, the laser measurements do not work well on a glass surface because part of the pulse is refracted through the glass and there is a weak return of the reflected ray. Thus the measurement keeps changing and is unreliable.



## 5. CONCLUSIONS AND RECOMMENDATIONS

### 5.1. Conclusions

In this research, we looked at the use of terrestrial IBM for creating a 3D model and a 2D model that can be used as a cadastral boundary in a slum environment, the results are very promising in terms of relative accuracy, time and costs incurred. This approach is revolutionary in that it can be done by a single person. The 3D model can be extracted primarily from geotagged images using a digital camera with an inbuilt GPS. However, reference measures are necessary for correcting scale errors and for improving the positional accuracy of the model.

The main challenge is the image acquisition exercise. This must be carried out carefully with high overlaps in adjacent datasets to ease the problem of co-registration between corresponding datasets.

The methods used to create the 3D and 2D models produced good quality models with relatively good accuracy.

#### 5.1.1. Answers to research questions

##### 1. *How will the entire area of interest be captured?*

A good quality camera should be used to capture high resolution images with a high overlap of approximately 80%. When taking the images along the corridors, forward facing photos should be taken ensuring both the ground and building facades are captured. Images taken in adjacent days should have a large area of overlap to ease in co-registration of the different models. Cluttered scenes are very difficult to avoid and thus multiple images should be taken so as to find more matches in the overlapping images.

##### 2. *How to create a 3D model of the slum*

The idea is to process the data as different blocks of images, considering time of image acquisition and also using an object based approach. The processing of images with little matches between them results in problematic point clouds with multiple disconnected blocks. Images with poor geoinformation should be given low horizontal and vertical accuracy so that the image orientation process can compute the calibrated new image positions more independent from their initial positions.

**3. *How can the 2D boundary of the slum be extracted from facades of the buildings, considering a problematic 3D model due to the characteristics of a slum?***

Automatic delineation of a 2D footprint from the horizontal and vertical planes in the slum environment is not feasible due to clutter, occlusions and very noisy point clouds. Furthermore defining the planes is near impossible. Manual digitizing in the point clouds can be used in this and the vertices of the polylines refined in the overlapping images.

**4. *How to determine the geometric accuracy of the models?***

Quality assessment and quality checks can be done in a point cloud in various ways. The first analysis is just a visual check. By just looking at the point cloud, misplaced blocks can be identified as well as noisy point clouds. Second an internal accuracy can be done by plane fitting in the facades of the buildings. In some cases, the facades are displaced and this can be checked using plane fitting. Finally, the most effective method is use of reference data. Data from GPS, orthophotos and maps can be used to check the positional accuracy of the models.

**5. *How to scale the models using Spike laser measurements?***

Horizontal and vertical reference measures were done in the facades of the buildings and used to scale the point clouds. These measurements were used as scaling constraints in the SfM process. To analyse the quality of the spike device different measurements were done on a plane surface. By taking multiple measurements to the same surface using different angles and distances for the laser to the target, these were compared to the reference measurements from a measuring tape. Horizontal and vertical measurements were done as well as area measurements to different surface materials (brick walls, wood, glass and metallic surfaces). Statistical analysis was then carried out.

**6. *How will the registration differences between the different point clouds be handled and then stitched together to one model?***

This involves automatic co-registration by use of a rigid transform between two overlapping point clouds. After the registration is done new exterior orientations can be computed and used to reprocess the block. Reference data can be used to correct inconsistencies not solved in the rigid transform.

## 5.2. Recommendations

The method used in the research was good enough to realise the objectives of the research. However, some challenges were experienced and lessons learnt. In future, the following should be addressed:

- To address the high accuracy level required in cadastral works, 3D ground control points should be used for absolute positioning.
- It is necessary to have larger overlaps between adjacent blocks during the image acquisition for the purpose of registration.
- During image acquisition, after switching on the camera, the operator should allow time for the camera GPS to initialise before taking the first image. He/she should wait until the geolocation on the GPS gives a fixed solution. Otherwise, the first few images will have no or poor geoinformation.
- Though use of fully automated methods for extraction of the 2D footprint in the slums is not practical, research should be done in developing a semi-automatic method that can be used, especially in large projects



## LIST OF REFERENCES

---

- Agarwal, S., Furukawa, Y., Snavely, N., Curless, B., Seitz, S. M., & Szeliski, R. (2010). Reconstructing Rome. *Computer*, 43, 40–47. doi:10.1109/MC.2010.175
- Amnesty International. (2009). Kenya: The unseen majority: Nairobi's two million slum-dwellers. Retrieved August 11, 2015, from <https://www.amnesty.nl/nieuwsporaal/rapport/kenya-unseen-majority-nairobi-s-two-million-slum-dwellers>
- Bay, H., Tuytelaars, T., & Van Gool, L. (2006). Surf: Speeded up robust features. *Lecture Notes in Computer Science*, 3951, 14. doi:10.1007/11744023\_32
- Bellekens, B., Spruyt, V., & Weyn, M. (2014). A Survey of Rigid 3D Pointcloud Registration Algorithms. *AMBIENT 2014, The Fourth International Conference on Ambient Computing, Applications, Services and Technologies. 2014.*, (c), 8–13.
- Besl, P., & McKay, N. (1992). A Method for Registration of 3-D Shapes. *IEEE Transactions on Pattern Analysis and Machine Intelligence*. doi:10.1109/34.121791
- Debevec, P. E., Taylor, C., & Malik, J. (1996). Modeling and rendering architecture from photographs: A hybrid geometry-and image-based approach. *Siggraph 96*, 1–10. doi:<http://doi.acm.org/10.1145/237170.237191>
- Fischler, M. a., & Bolles, R. C. (1981). Random sample consensus: a paradigm for model fitting with applications to image analysis and automated cartography. *Communications of the ACM*, 24(6), 381–395. doi:10.1145/358669.358692
- Furukawa, Y., & Ponce, J. (2010). Accurate, dense, and robust multiview stereopsis. *IEEE Transactions on Pattern Analysis and Machine Intelligence*, 32(8), 1362–1376. doi:10.1109/TPAMI.2009.161
- Girardeau-Montaut, D. (2015). cloud compare. Retrieved July 11, 2015, from <http://www.cloudcompare.org/>
- Haala, N. (2011). Multiray Photogrammetry and Dense Image Matching, 185–195.
- Hirschmuller, H. (2005). Accurate and Efficient Stereo Processing by Semi-Global Matching and Mutual Information. *Computer Vision and Pattern Recognition, 2005. CVPR 2005. IEEE Computer Society Conference on*, 2, 807–814 vol. 2. doi:10.1109/CVPR.2005.56
- IkeGPS. (2015). Spike | ikeGPS. Retrieved June 2, 2015, from <http://www.ikegps.com/spike/>
- Joshi, R. (2014). Automated 3D feature extraction for simple geometry buildings using images for GIS data collection Automated 3D feature extraction for simple geometry buildings using images for GIS data collection. *Faculty of Geo-Information Science and Earth Observation of the University of Twente (ITC)*.
- Li, Z., Chen, J., & Baltsavias, E. (2008). *Advances in Photogrammetry, Remote Sensing and Spatial Information Sciences: 2008 ISPRS Congress Book*. CRC Press. Retrieved from <https://books.google.com/books?id=-fQM3buoejC&pgis=1>
- Liebowitz, D., Criminisi, A., & Zisserman, A. (1999). Creating Architectural Models from Images. *Computer Graphics Forum*, 18(3), 39–50. doi:10.1111/1467-8659.00326

- Lorsakul, A. (2008). Point-cloud-to-point-cloud technique on tool calibration for dental implant surgical path tracking. *Medical ...*, 2–13. doi:10.1117/12.772257
- Lowe, D. G. (2004). Distinctive Image Features from Scale-Invariant Keypoints, *60*(2), 91–110.
- OpenStreetMap | Way: Mashimoni (48161267). (n.d.). Retrieved February 2, 2016, from <https://www.openstreetmap.org/search?query=mathare+nairobi#map=18/-1.26307/36.86192>
- Panchal, P. M., Panchal, S. R., & Shah, S. K. (2013). A Comparison of SIFT and SURF. *International Journal of Innovative Research in Computer and Communication Engineering*, *1*(2), 323–327.
- Pix4Dmapper. (2015). Pix4D UAV mapping photogrammetry software, Pix4Dmapper. Retrieved July 8, 2015, from <https://pix4d.com/products/>
- Remondino, F. (2011). Heritage recording and 3D modeling with photogrammetry and 3D scanning. *Remote Sensing*, *3*(6), 1104–1138. doi:10.3390/rs3061104
- Shahbazi, M., Sohn, G., Théau, J., & Ménard, P. (2015). Uav-Based Point Cloud Generation for Open-Pit Mine Modelling. *ISPRS - International Archives of the Photogrammetry, Remote Sensing and Spatial Information Sciences, XL-1/W4*, 313–320. doi:10.5194/isprsarchives-XL-1-W4-313-2015
- Snavely, N., Seitz, S. M., & Szeliski, R. (2008). Modeling the world from Internet photo collections. *International Journal of Computer Vision*, *80*(2), 189–210. doi:10.1007/s11263-007-0107-3
- Tam, G. K. L., Cheng, Z. Q., Lai, Y. K., Langbein, F. C., Liu, Y., Marshall, D., ... Rosin, P. L. (2013). Registration of 3d point clouds and meshes: A survey from rigid to Nonrigid. *IEEE Transactions on Visualization and Computer Graphics*, *19*(7), 1199–1217. doi:10.1109/TVCG.2012.310
- Tola, E., Strecha, C., & Fua, P. (2012). Efficient large-scale multi-view stereo for ultra high-resolution image sets. *Machine Vision and Applications*, *23*(5), 903–920. doi:10.1007/s00138-011-0346-8
- Turner, D., Lucieer, A., & Watson, C. (2012). An automated technique for generating georectified mosaics from ultra-high resolution Unmanned Aerial Vehicle (UAV) imagery, based on Structure from Motion (SfM) point clouds. *Remote Sensing*, *4*(5), 1392–1410. doi:10.3390/rs4051392
- Westoby, M. J., Brasington, J., Glasser, N. F., Hambrey, M. J., & Reynolds, J. M. (2012). “Structure-from-Motion” photogrammetry: A low-cost, effective tool for geoscience applications. *Geomorphology*, *179*, 300–314. doi:10.1016/j.geomorph.2012.08.021
- Zeng, H., Zhang, B., Mu, Z., & Wang, X. (2013). A Planar Metrology Method Based on Image Sequence. *Proceedings of the 2nd International Symposium on Computer, Communication, Control and Automation*, (3ca), 296–299. doi:10.2991/3ca-13.2013.74



# APPENDICES

---

## Appendix 1: Schuur Building at the UT

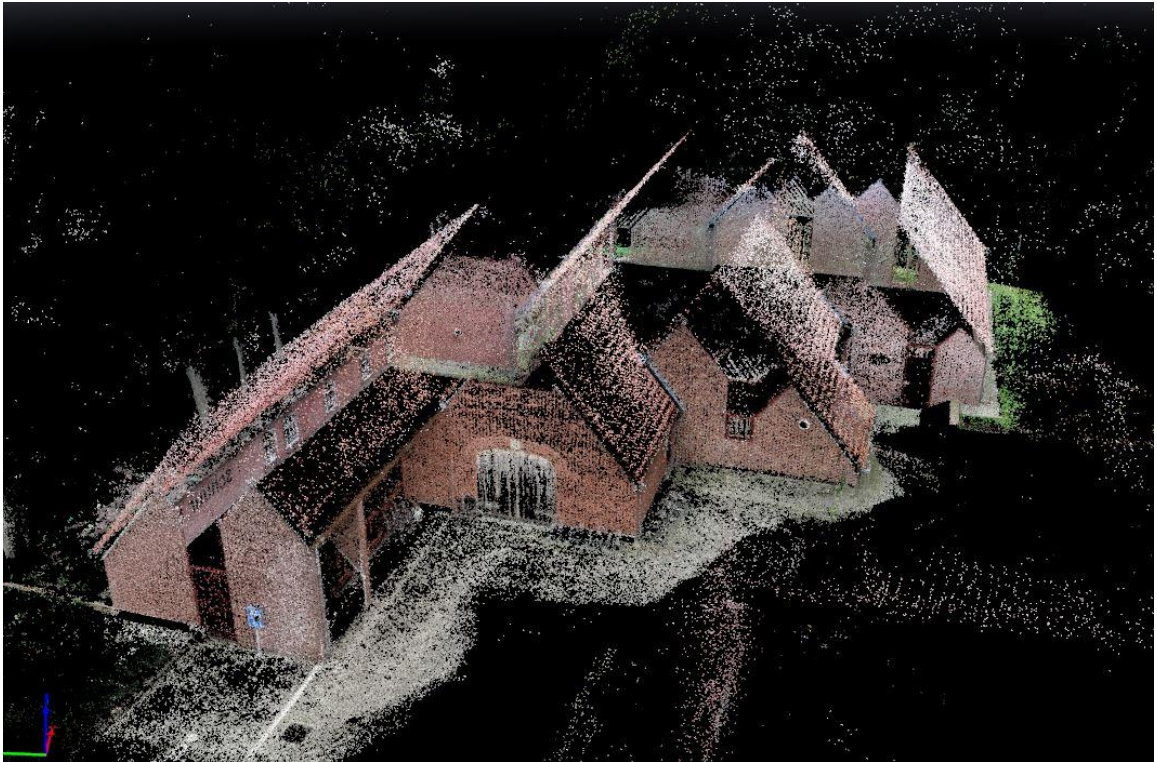


Figure 5.1: Point cloud of Schuur building

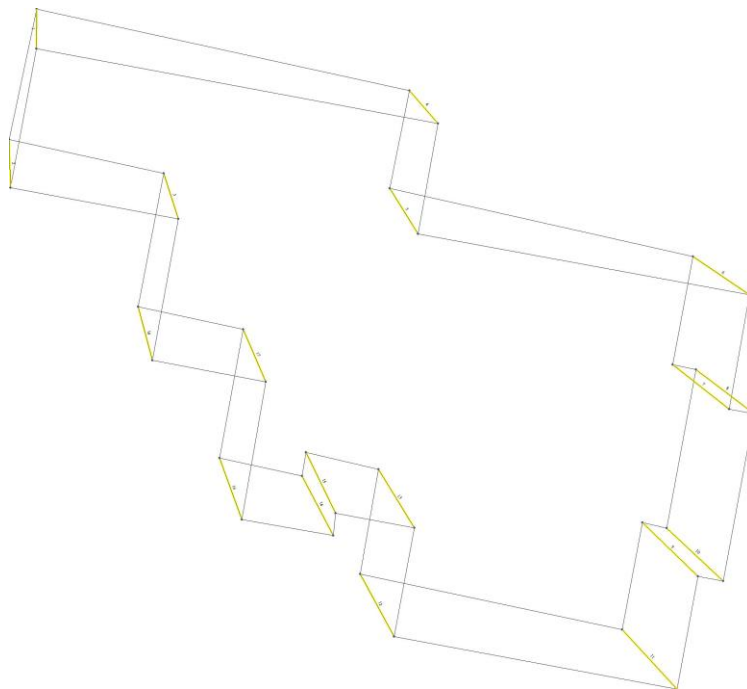


Figure 5.2: Comparison of 2D models

## Appendix 2: Comparison of 2D GCPs and 3D GCPs

Point Cloud_GPS(Reference)				Point Cloud (2D GCPs)				GPS -2D			D
Name	POINT_X	POINT_Y	POINT_Z	Name	POINT_X	POINT_Y	POINT_Z	dx	dy	dz	
GPS1	439.375	39.306	29.645	CP1	439.497	39.331	30.523	-0.12182	-0.02546	-0.87755	0.124449
GPS2	440.409	27.953	29.396	CP2	440.438	27.923	31.081	-0.02918	0.03007	-1.68533	0.041902
GPS3	441.85	53.308	29.353	CP3	442.005	53.156	29.547	-0.15541	0.15171	-0.1939	0.217184
GPS4	442.258	38.599	29.18	CP4	442.586	38.619	30.207	-0.32793	-0.01997	-1.02684	0.328537
GPS5	447.721	20.539	29.515	CP5	447.750	20.565	31.920	-0.02944	-0.02559	-2.40518	0.039007
GPS6	448.902	26.466	29.462	CP6	448.660	26.269	31.653	0.24228	0.19659	-2.19078	0.312005
GPS7	452.894	18.084	29.5	CP7	453.010	18.240	32.314	-0.11578	-0.15617	-2.8144	0.194409
GPS8	453.254	19.582	29.51	CP8	453.365	19.512	32.341	-0.11137	0.06985	-2.83083	0.131459
GPS9	454.894	42.085	29.218	CP9	454.822	42.019	30.620	0.071504	0.06625	-1.40161	0.097478
GPS10	455.755	17.744	29.262	CP10	455.756	17.664	32.271	-0.00055	0.08017	-3.00895	0.080172
GPS11	456.173	20.286	29.246	CP11	456.162	20.136	31.009	0.0106	0.149746	-1.76309	0.150121
GPS12	456.543	50.532	29.398	CP12	456.451	50.544	30.255	0.091646	-0.01227	-0.85678	0.092464
GPS13	461.02	40.601	29.085	CP13	460.935	40.749	30.964	0.085402	-0.1485	-1.87942	0.171306
GPS14	461.482	44.076	29.215	CP14	461.493	43.972	30.843	-0.01054	0.10386	-1.62844	0.104393
GPS15	465.33	18.704	29.394	CP15	465.298	18.685	32.777	0.032408	0.01894	-3.38339	0.037537
GPS16	466.366	24.236	29.257	CP16	466.334	24.202	32.354	0.032227	0.03378	-3.09664	0.046687
GPS17	468.028	23.85	29.418	CP17	468.009	23.813	32.627	0.019112	0.03707	-3.2093	0.041707
GPS18	471.377	42.052	29.534	CP18	471.312	42.042	31.842	0.064555	0.0097	-2.30791	0.06528

## Appendix 3: Spike measurements



Figure 5.3: Wall facade measurement



Figure 5.4: Wooden surface measurements



Figure 5.5: Metallic surface measurements



#### Appendix 4: Matlab Script for transformation

```
cd ('C:/School/Registered Pcs new/Day3/')
R=textread ('rotICP4.mat');
T=textread ('transICP4.mat');
EO_ini=textread ('Initial.txt');
[n, dim1]=size(EO_ini);

offset=[262000.000,9860000,1000];
EO_ini_short = EO_ini - repmat(offset,n,1);
EO_trans_short = R*EO_ini_short + repmat(T,1,n);
EO_trans=EO_trans_short'+repmat(offset,n,1);
save('EO_trans.txt','-ascii','EO_trans')
```